Journal of Medicinal Chemistry

Article

Cite This: J. Med. Chem. XXXX, XXX, XXX−XXX

pubs.acs.org/jmc

qFit-ligand Reveals Widespread Conformational Heterogeneity of Drug-Like Molecules in X-Ray Electron Density Maps

Gydo C. P. van Zundert,[†] Brandi M. Hudson,[‡] Saulo H. P. de Oliveira,[⊥] Daniel A. Keedy,[‡,#] Rasmus Fonseca,[§] Amelie Heliou,[∥] Pooja Suresh,[‡] Kenneth Borrelli,[†] Tyler Day,[†] James S. Fraser,[‡] and Henry van den Bedem*[,‡,⊥]

[†]Schrödinger, New York, New York 10036, United States

[‡]Department of Bioengineering and Therapeutic Sciences, UCSF, San Francisco, California 94158, United States

[§]Department of Molecular and Cellular Physiology, Stanford University, Stanford, California 94305, United States

[∥]LIX, Ecole Polytechnique, CNRS, Inria, Université Paris-Saclay, 91128 Palaiseau, France

[⊥]SLAC National Accelerator Laboratory, Stanford University, Menlo Park, California 94025 United States

Supporting Information

ABSTRACT: Proteins and ligands sample a conformational ensemble that governs molecular recognition, activity, and dissociation. In structure-based drug design, access to this conformational ensemble is critical to understand the balance between entropy and enthalpy in lead optimization. However, ligand conformational heterogeneity is currently severely underreported in crystal structures in the Protein Data Bank, owing in part to a lack of automated and unbiased procedures to model an ensemble of protein−ligand states into X-ray data. Here, we designed a computational method, *qFit-ligand*, to automatically resolve conformationally averaged ligand heterogeneity in crystal structures, and applied it to a large set of protein receptor−ligand complexes. In an analysis of the cancer related BRD4 domain, we found that up to 29% of protein crystal structures bound with drug-like molecules present evidence of unmodeled, averaged, relatively isoenergetic conformations in ligand−receptor interactions. In many retrospective cases, these alternate conformations were adventitiously exploited to guide compound design, resulting in improved potency or selectivity. Combining *qFit-ligand* with high-throughput screening or multitemperature crystallography could therefore augment the structure-based drug design toolbox.

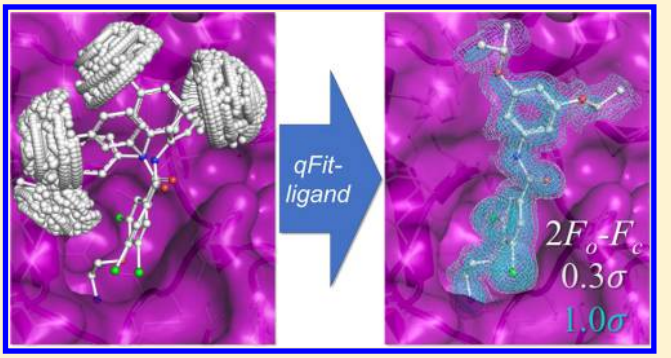

INTRODUCTION

Ligands and their protein receptors sample an ensemble of conformations in solution. The energetic contribution of conformational entropy plays a critical role in receptor−ligand molecular recognition,[1,2] but the ensemble of conformations that determines the free energy of binding, activity, and dissociation often remains poorly characterized. The majority of three-dimensional protein structures are single, static models obtained from X-ray crystallography by averaging over the unique conformations in the unit cells. Crystallographic atomic displacement parameters (ADP) quantify harmonic displacements from average atomic positions but are adversely affected when unmodeled discrete alternate conformations overlap. By their nature, such static, harmonic models cannot rationalize molecular attributes that rely on dynamic, anharmonic displacements of atoms.[3,4] Revealing discrete conformations[5−7] that are more fully representative of the receptor−ligand conformational ensemble from X-ray electron density maps would overcome this limitation and create new opportunities to address open questions in chemical and structural biology. For example, such models might help to provide a structural basis for on-pathway conformational intermediates in substrate binding or release detected by NMR.[8,9]

Additionally, an incomplete picture of receptor−ligand structural dynamics impedes structure-based drug design. While overall binding affinities measured in solution report on a receptor−ligand ensemble, the structure−activity relationships are often informed by static models for further optimization, with some exceptions that incorporate flexibility.[10] During small-molecule optimization, even minor chemical changes can lead to apparently altered binding modes that are unforeseen due to the limitations of conventional X-ray structural models, frustrating design[11,12] (Figure 1A). One hypothesis to explain how subtle modifications cause a switch to a second binding pose is that the unmodified ligand samples the second pose at low, but potentially detectable, occupancy (Figure 1B). Examples where

Received: August 15, 2018
Published: November 20, 2018

DOI: 10.1021/acs.jmedchem.8b01292
J. Med. Chem. XXXX, XXX, XXX−XXX

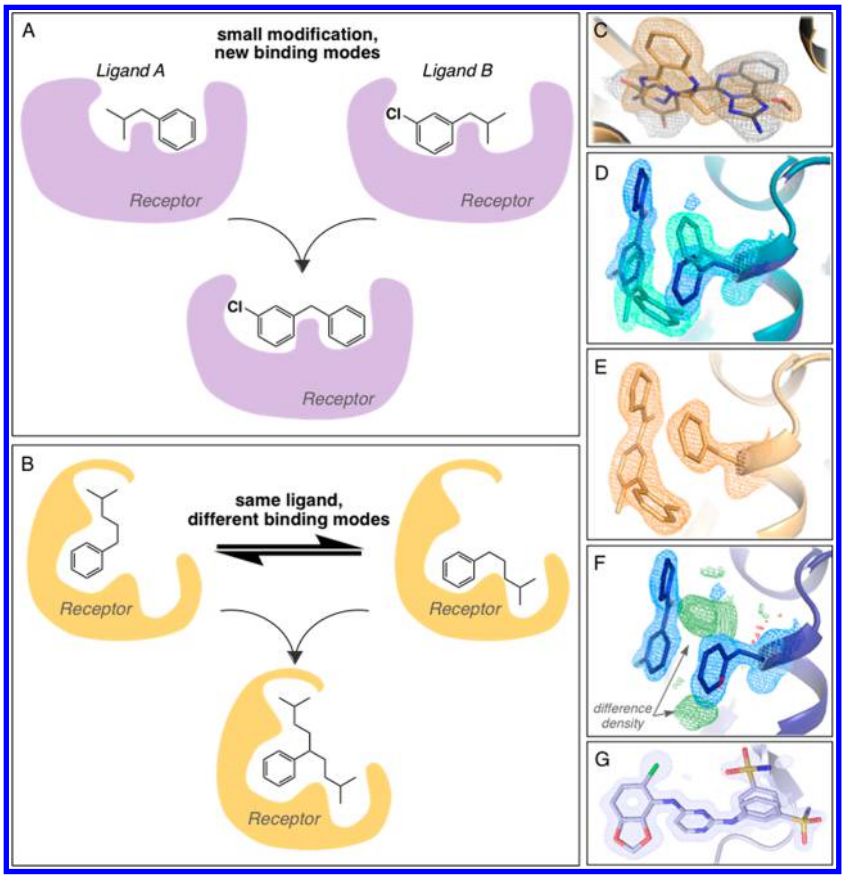

Figure 1. Ligand structural dynamics and minor changes during fragment optimization lead to new binding modes and drive drug design. (A) Subtle changes in chemical structure of ligands can impose new binding modes. (B) Near isoenergetic receptor−ligand conformations exchange in dynamic equilibrium in crystal structures. These conformations can inform the design of a ligand with higher affinity. (C) Hsp90 inhibitors in gray (PDB 4CWO) and gold (PDB 4CWN). (D) Subtle changes in chemical structures lead to changes in binding pose for Lp-PLA2, changing the course of design (PDBs 5JAL, 5JAO). (E) New Lp-PLA2 inhibitor designed as a result of observed alternate binding poses of fragments (PDB 5JAP). (F) Evidence of difference density in X-ray crystal structure of Lp-PLA2 fragment shows alternate binding poses pre-exist at low occupancy (PDB 5JAL). (G) Alternate conformations exploited in the design of EphB4-binding ligands (PDB 2VWX). Electron densities are shown at 1.5σ. Positive (green) and negative (red) difference densities in part F are shown at +3.0σ and −3.0σ, respectively.

subtle changes in chemical structure of the ligand led to different binding modes are abundant. Fragment optimization of CDK8 inhibitors revealed that small modifications led to a new binding mode, which was exploited to develop potent and selective inhibitors.[13] Dramatically different binding modes as a result of minor changes in the chemical structure of the ligand are also illustrated by Hsp90 and PTR1 inhibitors. In the course of structure-based optimization of Hsp90 inhibitors, Casale and co-workers observed a flipped binding mode of the ligand in the crystal structure, leading them to change the direction of design toward a low nanomolar compound (Figure 1C).[14] In PTR1, compounds that presumably could not be accommodated by the binding site ultimately led to a boost in affinity, owing to altered binding modes.[14,15] In human lipoprotein-associated phospholipase A2, two related ligands (Figure 1D) that explored distinct subpockets were merged into a more potent ligand (Figure 1E).[16] These selected examples highlight both the perils of design based solely on an initial ligand pose but also how the fortuitous discovery of alternate poses can create new opportunities for design. It is possible that some of these "new" binding poses pre-exist as alternative conformations at slightly higher energies than the conformation modeled into the conventional X-ray structure. Many of those are infrequently sampled due to high energy differences and fall below the detection level in the maps. However, some of these conformations may be evident in electron density maps but at levels that are frequently ignored in modeling.

Indeed, in the phospholipase example above, the presence of difference electron density suggested that multiple conformations might have been sampled in at least one of the smaller ligands (Figure 1F). This view posits that degeneracies in ligand binding modes can also be accessed by small modifications of the ligand chemical structure that shift the receptor−ligand equilibrium ensemble. This hypothesis is supported by additional anecdotal examples, such as long time-scale molecular dynamics (MD) simulations of trypsin, in which both the ligand and receptor adopt many stable configurations.[17] Experimentally, multiple conformations can be present in X-ray electron density, as in HDAC6, where many related ligands were modeled in multiple conformations in concert with distinct conformations of the receptor.[18] In other cases where the alternate conformations have been experimentally revealed, they have been exploited to improve affinity. For example, X-ray crystallography revealed alternate conformations for singly substituted EphB4 ligands that inspired the creation of bis-substituted ligands with increased potency (Figure 1G).[19] NMR measurements of conforma-

DOI: 10.1021/acs.jmedchem.8b01292
J. Med. Chem. XXXX, XXX, XXX−XXX

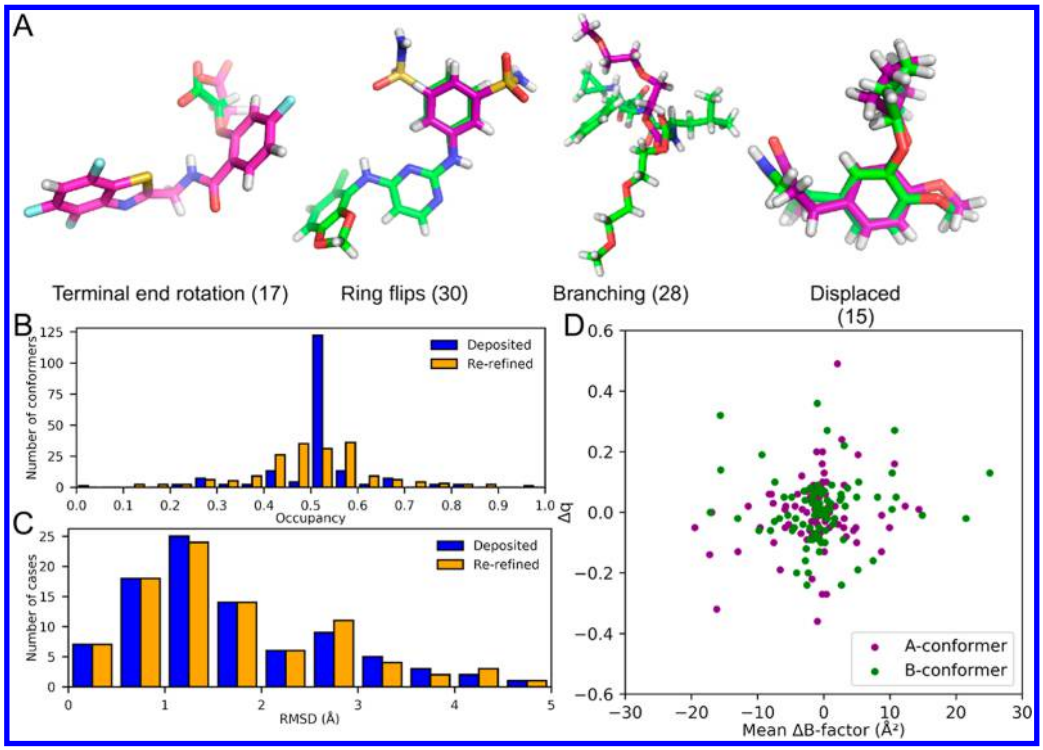

Figure 2. Benchmark statistics. (A) Categories of alternate conformations present in the benchmark. (B) Conformer occupancies pre- (blue) and post- (orange) rerefinement. (C) Ligand A to B conformer RMSD, pre (blue) and post (orange) rerefinement. (D) Occupancy shift versus mean *B*-factor difference after rerefinement.

tional heterogeneity for ligands generated against the antibacterial target LpxC uncovered a larger cryptic envelope that was filled by larger, more potent ligands.[20] Collectively, these examples suggest that multiple ligand poses are likely energetically accessible for many proteins. Fully realizing the potential of this phenomenon in structure-based design, exemplified by EphB4 and LpxC inhibitors, requires reliable characterization of pre-existing conformational heterogeneity (Figure 1B) of ligand−receptor complexes.

While protein conformational heterogeneity has been automatically and systematically characterized in X-ray crystallography data,[7,21−24] ligand conformational heterogeneity is less explored. Various software algorithms can identify and build ligands into electron density maps without human intervention;[25−30] however, these approaches typically provide several top scoring ligand conformations at unit occupancy. While in principle the user can select multiple candidate conformations for the final model, none of these approaches consider an ensemble of alternate conformations from the outset. Moreover, they may build unrealistic conformations that incorrectly fit into the ensemble-averaged electron density.[31] Despite the importance of low occupancy alternative conformations in biochemical function and ligand design, statistical measures for monitoring the fit of ensemble models to data are less developed than for single conformer models.

Here, we present a new, automated approach based on *qFit*,[22,23] called *qFit-ligand*, to create parsimonious multiconformer ligand models in crystallographic electron densities. We first surveyed the PDB to investigate ligand heterogeneity in current crystal structures and selected a diverse, curated benchmark set of pharmaceutically relevant protein targets with alternate ligand conformations across a wide range of resolution and occupancy (Supporting Information, Table S1). We found that *qFit-ligand* can detect alternate conformations at occupancies down to 20%, even at relatively modest resolutions of 2.0 Å. We then applied our method prospectively to all cases of the *Drug Design Data Resource* (D3R, drugdesigndata.org), a subset of the *Twilight Database*,[32] and all PDB entries for the bromodomain-containing protein 4 (BRD4), revealing unmodeled alternate conformations in 29% of the cases for the latter. To evaluate the quality of our multiconformer ligands, we calculated *R*-factors and ligand energies relative to a single conformer ligand model. Our results indicate that *qFit-ligand* is a powerful, efficient, and user-friendly tool to model and discover alternate ligand conformations.

RESULTS

Creating a Benchmark Set of True Positive Ligand Alternative Conformations from the PDB. To estimate the prevalence of multiconformer ligands in crystal structures, we surveyed all 130054 PDB entries as of June 2017 that contained noncovalently bound ligands with more than 15 non-hydrogen atoms in their X-ray crystal structure. This resulted in 44620 PDB entries totaling 133724 ligands. Of those, 2611 ligands, or less than 2% (1078 unique ligand codes), distributed over 1845 PDB entries, consisted of two or more alternate conformations (Supporting Information, Materials and Methods, Figure S1). Many of these molecules are common crystallographic additives (PEG, cholesterol, etc.) or metabolites (ATP, NADPH, etc.). We therefore manually curated a true positive benchmark set of receptors of pharmaceutical interest containing multiconformer, drug-like molecules. Cases where ligands adopted entirely different binding modes, such as flipped ligands, were discarded. This resulted in 90 crystal structures that could be stably refined

DOI: 10.1021/acs.jmedchem.8b01292
J. Med. Chem. XXXX, XXX, XXX−XXX

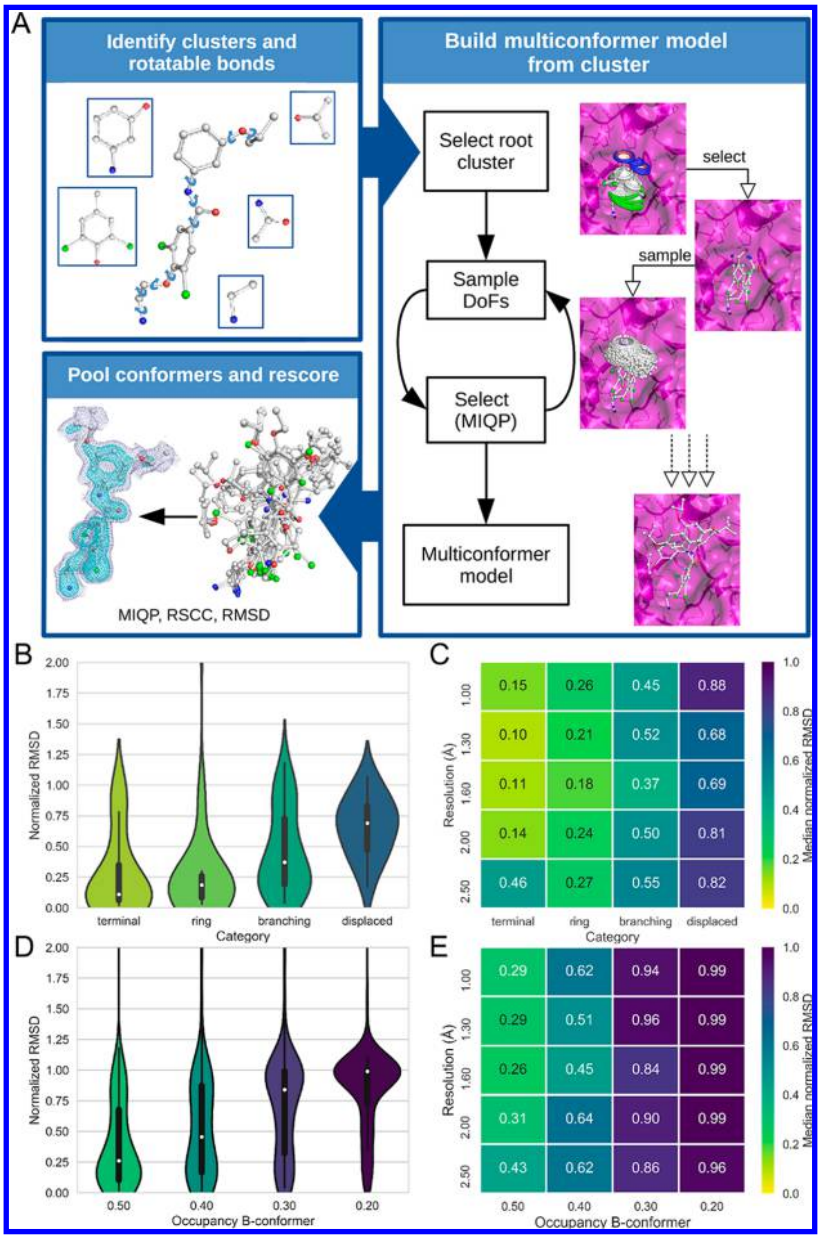

Figure 3. *qFit-ligand* workflow and statistics on synthetic data. (A) Rigid clusters are defined as rings or terminal ends, and rotatable bonds as any bond that is not part of a ring. The local search finds possible positions and orientations of each cluster in the binding site, avoiding steric clashes with the protein. As clusters are joined, torsions and degrees of freedom are sampled. Up to five ligand conformations that best match the ligand density are selected and combined with the protein model to give a final ligand multiconformer model. (B) Violin plot of categories at 1.60 Å resolution and occupancy 0.50 across 90 test cases. The white dot represents the median, the bold center line represent the interquartile range (IQR), and the thin center line represents the percentile range 25th −1.5 IQR to 75th +1.5 IQR. Lower nRMSD is better. (C) Heatmap of category vs resolution at 0.50 occupancy. Lower nRMSD is better. (D) Violin plot for representative resolution 1.60 Å and 0.50/0.50 occupancy at optimal parameters. (E) Heatmap of normalized RMSD at optimal parameters (resolution vs occupancy).

against the deposited structure factors and CIF restraints files (Supporting Information, Table S1).

We apportioned the conformational heterogeneity of ligands in our benchmark set into four categories (Figure 2A): terminal end flips, where only terminal atoms are flipped/rotated, ring flips where a ring system is flipped, usually by 180°, branching ligands, where a side chain or branch of a ligand has an alternate conformation, and displaced ligands, where all atoms are at least slightly displaced in combination with differences in their internal degrees of freedom. The benchmark set heavily overrepresented 50/50 occupancy splits (Figure 2B), reflecting a historical tendency against refining occupancies in favor of refining ADPs only. Inaccurate 50/50 occupancy splits do not inform on which conformation represents the dominant binding mode, which is often critical information for design decisions in lead optimization. Rerefinement with PHENIX[33] substantially broadened the distribution (Figure 2B). Unlike the occupancies, the RMSD between alternate conformations was similar after rerefinement (Figure 2C). Interestingly, we observed no correlation between occupancy shift and difference in mean *B*-factor (Figure 2D). This result is in contrast to earlier reports,[34,35] likely owing to improvements in refinement software.

DOI: 10.1021/acs.jmedchem.8b01292
J. Med. Chem. XXXX, XXX, XXX−XXX

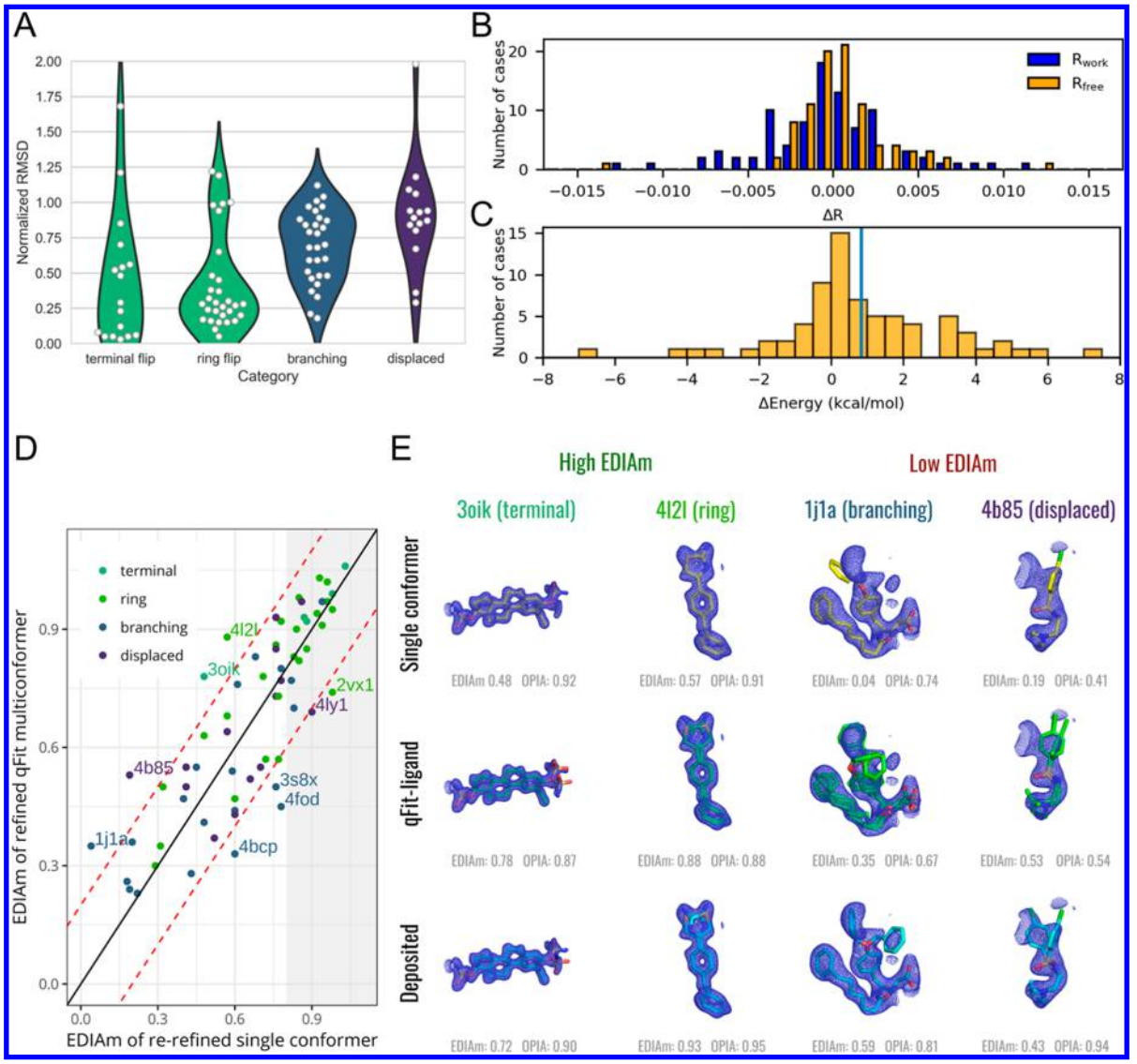

Figure 4. Electron density support measures and energetics of *qFit-ligand* multiconformers are similar to those of single-conformer models for the benchmark set while reporting on conformational heterogeneity. (A) nRMSD distributions by category of conformational heterogeneity. The nRMSD of terminal end flips was determined from only atoms affected by the dihedral changes. Lower nRMSD is better. (B) Histogram of R_{work} and R_{free} differences between refined *qFit-ligand* models and single conformer structures. Negative values indicate a lower R for refined *qFit-ligand* models. (C) The distribution of occupancy-weighted, ligand internal energies of *qFit-ligand* multiconformer ligands relative to single "A" conformation. Negative values indicate that the multiconformer ensemble has lower internal energy than the single benchmark "A" conformation. Positive values indicate the multiconformer ensemble has higher internal ligand energies. (D) Ligand EDIAm scores for rerefined single conformer models against automatically refined *qFit-ligand* multiconformer models. Higher EDIAm scores are better, with scores greater than 0.8 indicating that the model is well-supported by the density (shaded area for single conformer models). (E) Examples where the ligand EDIAm was improved by modeling alternate conformations with *qFit-ligand*. The $2mF_o - DF_c$ maps are shown in blue at a contour level of 1σ.

Developing the *qFit-ligand* Algorithm and Calibration against Synthetic Data. We designed the *qFit-ligand* algorithm to iteratively explore a vast conformational space to determine a parsimonious ensemble of up to five occupancy-weighted conformations that, collectively, optimally fit the electron density (Figure 3A and Supporting Information, Materials and Methods, Figure S2). Briefly, *qFit-ligand* takes as input a refined, single conformation receptor−ligand structure in PDB format, and a $2mF_o - DF_c$ density map. It first determines rotatable bonds and rigid groups of atoms within the ligand (Supporting Information, Materials and Methods, Figure S2). Starting from each rigid group, *qFit-ligand* performs a local, six-dimensional translational and rotational search in the rigid group's neighborhood, selecting up to five occupancy-weighted candidate positions that, collectively, minimize the real-space density residual of the rigid group. In subsequent steps, *qFit-ligand* iteratively grows the rigid group by exhaustively sampling increments of several torsion angles simultaneously while avoiding collisions with the receptor. At each step, it selects up to five occupancy-weighted conformations by again minimizing the density residual. This is repeated until all torsion angles are determined and the full ligand is built up. The maximum number of conformations generated by *qFit-ligand* at this stage is five times the number of rigid groups. The final occupancy-weighted, multiconformer ensemble is selected from this pool by combining cross-correlation, geometric, and density residual measures. The

DOI: 10.1021/acs.jmedchem.8b01292
J. Med. Chem. XXXX, XXX, XXX−XXX

ligand multiconformer ensemble is then combined with the receptor and refined with *phenix.refine*.

We calibrated *qFit-ligand* on synthetic data calculated from the benchmark set at varying resolutions and occupancies (Supporting Information, Materials and Methods, Figure S3). To create starting models we deleted the alternate "B" conformation of the ligand, set the occupancy of the "A" conformation to 1.0, and rerefined against the deposited structure factors to reposition the "A" conformation as the only modeled conformation.

We first determined optimal sampling parameters for *qFit-ligand*, balancing accuracy of the results and computational demands, measured by the minimum normalized RMSD (nRMSD, Supporting Information, Materials and Methods, Figure S3) between *qFit-ligand* generated conformations and the benchmark B conformation. RMSDs between the A and B conformers range from 0.22 to 4.86 Å across the benchmark set. nRMSD controls for this large variation by normalizing the RMSD between *qFit-ligand* generated conformations and the B conformer by the RMSD between A and B. nRMSD values range from 0 to 1, with values closer to 0 indicating better performance. To compare performance, we report the median nRMSD of the benchmark set for different resolutions and occupancies. Our analysis suggested that sampling two torsion angles simultaneously at 6° intervals gave the best result across resolutions and occupancies while limiting computational costs (Supporting Information, Figure S4).

Benchmarking *qFit-ligand* showed performance differences across category, resolution, and true occupancy. We evaluated the performance of *qFit-ligand* for each category of conformational heterogeneity (Figure 3B,C). At a resolution of 1.60 Å and equal occupancies for the A and B conformer, the median nRMSD is 0.11 for terminal end flips, 0.18 for ring flips, 0.37 for branched ligands, and 0.69 for displaced ligands (Figure 3B). Unsurprisingly, *qFit-ligand* performance decreased with increasing complexity of conformational heterogeneity.

The resolution dependence is more complex, however, with better performance of *qFit-ligand* at an intermediate resolution of 1.60 Å (Figure 3C,E). We attribute this to more sharply defined density peaks at high resolutions relative to intermediate resolutions. Undersampling of conformations during ligand building can result in failure to accurately hit the density peaks at high resolution, thereby leading to suboptimal scores of electron density-based measures.

The performance of *qFit-ligand* is sensitive to the occupancy of the alternate conformation, indicated by an increasing median nRMSD for lower occupancies of the B conformation (Figure 3D,E). At occupancies of 0.2 and below, the alternate conformer was rarely detected at any resolution. While *qFit-ligand* samples conformations close to the alternate conformer, evidenced by favorable (low) nRMDS before final rescoring (Supporting Information, Figure S4), selecting them at low occupancies would increase the false positive rate (data not shown).

Finally, note that the *qFit-ligand* multiconformer ensemble *collectively* explains the density best. In virtually all cases, density profile contributions from all ligand conformers are required to match the experimental profile. Overlapping ensemble members evaluated in isolation generally return suboptimal density fitting statistics.

***qFit-ligand* Reidentifies Low Energy Alternative Conformations in Experimental Data.** Next, we applied our method to the experimental benchmark data set for cases with resolution better than 2.20 Å (73 cases), with only the "A" conformation retained in the rerefined starting model (Figure 4). *qFit-ligand* performance with real data followed the trend we observed with simulated data: localized conformational disorder like terminal end flips and ring flips were determined with higher accuracy than branched or displaced disorder. In the case of terminal ends, only one or two atoms report on the distance between alternate conformations, but the nRMSD is dominated by small coordinate shifts distributed over the entire ligand. Despite a median nRMSD of 0.56 for terminal ends, the median nRMSD for only the "reporting" atoms is less than 0.30 (Figure 4A; all RMSDs reported in Supporting Information, Figure S5). Consequently, 13 out of 17 terminal end flip *qFit-ligand* results were sufficiently accurate to recognize the benchmark alternate conformer. Similarly, *qFit-ligand* determined ring rotations to within a median nRMSD of 0.27. However, the median nRMSD for branched cases is 0.78 and for displaced cases is 0.87. If we conservatively designate a *qFit-ligand* result with more than one conformation and nRMSD > 0.6 as a false positive (Supporting Information, Figure S6), the false positive rates for each category are 29% (terminal flip), 14% (ring flip), 67% (branching), and 85% (displaced) (*see* Discussion *section regarding false positives*).

The distribution of R_{free} values of fully automated refined *qFit-ligand* models were nearly identical to that of the single conformer ligand models (*qFit-ligand* $\bar{x}$ = 0.2043, single conformer $\bar{x}$ = 0.2048, p-value = 0.46, two-sided t test) and statistically indistinguishable from the deposited, manually curated multiconformers ($\bar{x}$ = 0.2038, p-value = 0.51) (Figure 4B, Supporting Information, Figure S7, Table S2). The *qFit-ligand* multiconformer models improved (worsen) R_{free} in 53% (47%) of cases compared to single conformer ligand models.

The R_{free} value alone is generally not sufficiently sensitive to detect if a multiconformer model is, collectively, supported by the electron density. Therefore, as an independent validation in addition to the RSCC in the *qFit-ligand* algorithm, we calculated the electron density support for individual atoms (EDIAm) score.[36] The EDIAm score quantifies how well a group of atoms is supported by the electron density (Materials and Methods). EDIAm scores indicated that the *qFit-ligand* models improve agreement with the electron density in 63% of cases compared to a single conformer model (Figure 4D) and overall were within 0.2 of those of single conformer models. In cases where deposited models were well-supported by the electron density (EDIAm > ~0.8), *qFit-ligand* models generally increased EDIAm compared to single conformer models, in some cases even improving the deposited model (Figure 4D,E, 3oik). Unsurprisingly, EDIAm scores correlated with the categories of conformational disorder; branched or displaced ligands had lower EDIAm scores. Nonetheless, even in those challenging cases, automated *qFit-ligand* multiconformers EDIAm scores are on par with those of single-conformer models while alerting to the presence of conformational heterogeneity (Figure 4E, right-hand panels; Supporting Information, Figure S15). We emphasize that R_{free} and EDIAm values from fully automated modeling generally improve with manual refinement.

To further evaluate the quality of *qFit-ligand* multiconformer models, we examined internal ligand energies, ignoring interactions with the receptor. Although *qFit-ligand* does not observe restraints in modeling, the quality of *qFit-ligand* multiconformer models as measured by their internal energy was excellent. We found a median conformationally averaged

DOI: 10.1021/acs.jmedchem.8b01292
J. Med. Chem. XXXX, XXX, XXX−XXX

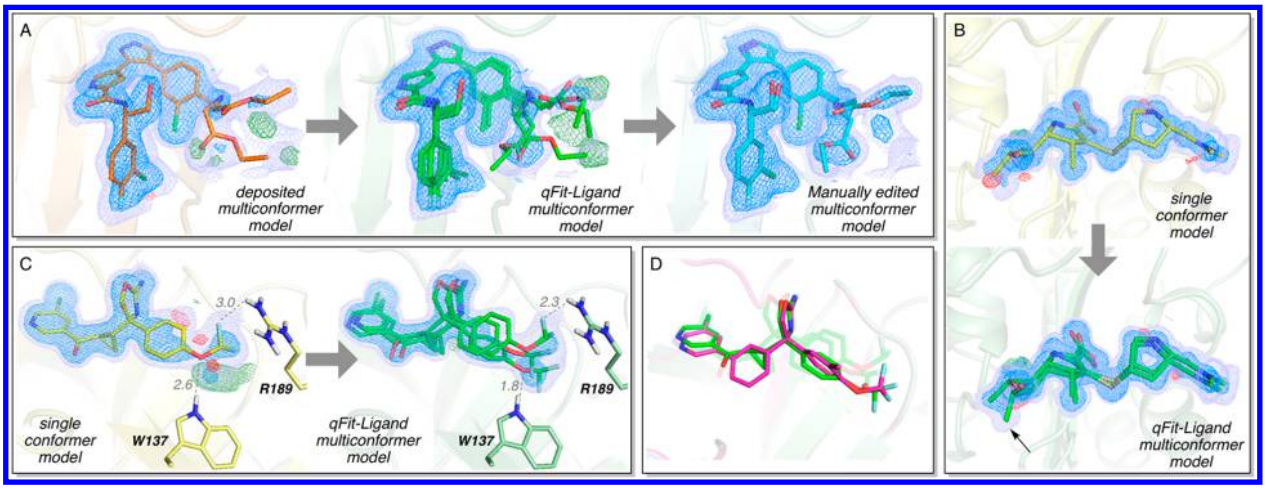

Figure 5. Prospective discovery of additional conformations and recovered conformations from the D3R and *Twilight* data set. (A) The deposited multiconformer model, *qFit-ligand* multiconformer model, and manually edited multiconformer model of ERK2 (PDB 4FV3; new PDB 6DMG). (B) Single conformer and *qFit-ligand* multiconformer models of *Serratia fonticola* carbapenemase E166A mutant with the acylenzyme intermediate of meropenem (PDB 4EV4; new PDB 6DMH). (C) Prospective application of *qFit-ligand* to inhibitor 5T5 of BACE-1 (PDB 5EZX; new PDB 6DMI). Single conformer and *qFit-ligand* multiconformer models shown. (D) Overlay of multiconformer model of inhibitor 5T5 (green) with inhibitor 5T6 (magenta) (PDB 5EZZ). Electron densities are shown at 1.5σ (blue) and 0.3σ (purple). Positive (green) and negative (red) difference densities are shown at +3.0σ and −3.0σ, respectively. All structures shown have been refined using Phenix.

excess energy of only 0.35 kcal/mol (Supporting Information, Figure S16, Table S2,), i.e., q*Fit-ligand* multiconformer models were, on average, nearly indistinguishable from that of the rerefined single "A" conformation in our benchmark set. Interestingly, automatically building a *qFit-ligand* multiconformer model in some cases substantially reduced the ligand energy compared to the single "A" conformation. For example, for acyliminobenzimidazole inhibitor 36 in complex with human anaplastic lymphoma kinase,[37] a series of concerted dihedral angle changes resulted in conformations that better fit the density and reduced the energy by nearly 7 kcal/mol (Supporting Information, Figure S8). This suggests that a ligand can accumulate strain energy when it is forced into an averaged conformation to fit the density. On the other hand, the distribution of ligand excess energies suggests that ligands also access higher energy conformations, within a few kcal/mol from the single conformation (Figure 4D). Indeed, ligands generally may not bind in the lowest energy conformation or even adopt a local minimum.[38] Favorable noncovalent interactions with the receptor, buried hydrophobic surfaces, or desolvation of ordered waters in the binding pocket can overcome penalties of strained conformations.[39,40] Thus, alternate conformations, even at elevated ligand energies, may reduce the free energy of the receptor−ligand complex.

***qFit-ligand* Discovers New Alternate Conformations in the D3R and the *Twilight* Databases.** For prospective discovery, we first applied *qFit-ligand* to the 145 crystal structures in the D3R data set, a high-quality collection of manually curated protein−ligand crystal structures ranging in resolution from 1.26 to 2.75 Å, designed for validation and improvement of methods in computer-aided drug design. Of the 10 crystal structures in the D3R data set with alternate ligand conformations, *qFit-ligand* recovered seven to within a median nRMSD of 0.24. Four of these overlap with our benchmark (PDB 4FV3, Figure 5A, and PDBs 4EK6, 4EK8, 4Y6D). We ranked all *qFit-ligand* multiconformer ligands using the Fisher *z*-transformation, a cross-correlation based metric which measures if alternate conformations are supported by the electron density (Materials and Methods). Three of the top four ranked ligands already had a modeled alternate conformation, and six out of seven recovered multiconformer ligands ranked within the top 20, indicating that the Fisher-*z* transformation is an effective ranking measure. A new alternate ligand conformation was uncovered by *qFit-ligand* in the crystal structure of the E166A mutant of *Serratia fonticola* carbapenemase (PDB 4EV4; new PDB 6DMH) from the D3R data set (Figure 5B). The terminal propanol functional group of a bound meropenem intermediate adopts a previously undetected conformation. Thus, *qFit-ligand* recovered 70% of ligand alternate conformations and even revealed a new alternate conformation in highly scrutinized experimental data (*qFit-ligand* multiconformer models of prospective cases can be found in Zenodo; DOI: 10.5281/zenodo.1256262).

We also applied *qFit-ligand* to a subset of the *Twilight* data set. The *Twilight* data set represents ligand structures in the PDB poorly supported by the electron density map, potentially indicating conformational disorder in the map, or incorrectly modeled ligands. We applied *qFit-ligand* to ligands in the *Twilight* database with 15−36 non-hydrogen atoms, resolutions better than 2.0 Å, and a correlation coefficient higher than 0.6, resulting in 2379 cases over 1168 PDB entries, which we ranked by Fisher *z*-score to identify "hits" of unmodeled, alternate conformations (Supporting Information, Table S3). We proceeded by manually inspecting the top 10% of cases.

In many cases, the electron density near the ligand was severely disordered, consistent with the intent of the *Twilight* database to flag questionable models of ligands. While *qFit-ligand* suggested alternate conformations, their validity could not unambiguously be confirmed using electron density measures. Nonetheless, in some instances, significantly improved receptor−ligand interactions signified plausible alternate ligand conformations (Supporting Information, Figures S9, S10, S11).

However, for several crystal structures, *qFit-ligand* unambiguously detected alternate ligand binding conformations. For example, in the crystal structure of BACE-1, *qFit-ligand* finds three conformations (occupancies of 0.32/0.36/0.32) of inhibitor 5T5 (PDB 5EZX; new PDB 6DMI) (Figure 5C).

DOI: 10.1021/acs.jmedchem.8b01292
J. Med. Chem. XXXX, XXX, XXX−XXX

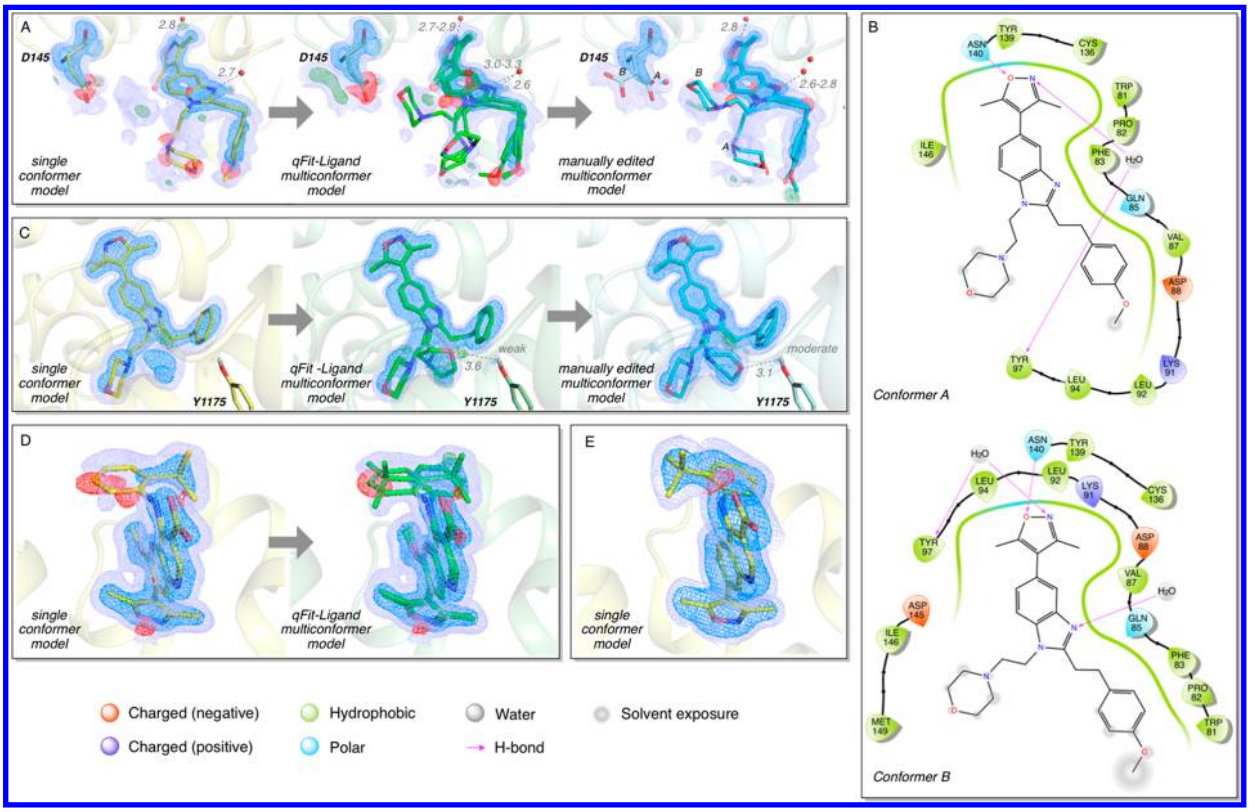

Figure 6. Prospective application of *qFit-ligand* to BRD compounds (A) Single conformer crystal structure, *qFit-ligand* multiconformer and manually edited multiconformer models including alternate conformations of Asp145 and compound BDOIA383 bound to BRD4 (PDB 5CFW; new PDB 6DMJ). (B) Protein−ligand interactions of the major, crystal-contact stabilized "A" and minor "B" BDOIA383 conformations of the final *qFit-ligand* model (A). (C) Single conformer crystal structure, *qFit-ligand* multiconformer and manually edited multiconformer models of a isoxazolyl-benzimidazole ligand bound to CBP BRD (PDB 4NR5; new PDB 6DMK). (D) Single conformer and *qFit-ligand* multiconformer models of ligand 9BM bound to BRD4 (PDB 4BW3; new PDB 6DML). Viewing orientation differs from parts A and C to clearly show ligand alternate conformations. (E) Ligand S5B's single binding conformation in BRD2 (PDB 4AKN). Electron densities are shown at 1.5σ (blue) and 0.3σ (purple). Positive (green) and negative (red) difference densities are shown at ±3.0σ. Distances in Ångstroms.

These conformations show the potential to engineer a ligand that can accommodate strong hydrogen bonding interactions to R189 and W137. In the single conformer model, one of the difluoromethoxy fluorines of the ligand and the amino group of R189 interact weakly through a 3.0 Å hydrogen bond.[41] Our multiconformer model shows that the ligand can adopt a position where strong hydrogen bonding between these groups occur (i.e., shorter contact distances), although at the expense of sacrificing a favorable hydrogen bonding interaction to W137. In addition, one of the *qFit-ligand* conformations turns a nonideal hydrogen bond geometry in the crystal structure between the difluoromethoxy oxygen and amino group of W137 into an ideal geometry. Strikingly, the difluoromethoxy group of BACE-1 inhibitor 5T6 (PDB 5EZZ) has a binding conformation that exploits this same hydrogen bonding interaction with W137 sampled by 5T5 at low occupancy (Figure 5D).[42] These insights could be used to create a new ligand with branching substituents that can simultaneously form strong hydrogen bonding interactions with R189 and W137 in hopes of increasing binding affinity.

***qFit-ligand* Identifies Widespread Conformational Heterogeneity in BRD4 Ligand.** In another notable example from the *Twilight* data set, *qFit-ligand* identified a minor, unmodeled population of inhibitor compound BDOIA383 bound to bromodomain-containing protein 4 (BRD4), a BET (bromodomain and extra terminal domain) and BRD (Figure 6A, PDB 5CFW; new PDB 6DMJ). BRDs are small, epigenetic "readers", which recognize and bind histone acetylated lysine (AcK).[43] BRDs can thereby epigenetically control gene transcription and have recently emerged as important drug targets.[44] The human genome contains 61 BRDs, distributed over 46 diverse proteins.[43] Several potent small-molecule inhibitors for BRD4 have been structurally characterized, but designing modulators selective between BRD4 and CREB binding protein (CBP) has proved challenging.[45−47]

The BRD4-BDOIA383 example highlights how alternate conformations can expose molecular surfaces away from the primary recognition site that could be exploited for selectivity. Inspection of the major population of BDOIA383 bound to BRD4 revealed that it is stabilized by a crystal contact between the BDOIA383 morpholine oxygen and the K91 carbonyl (Figure 6A). By contrast, the minor conformation does not engage in crystal contacts and buries nearly 6% more ligand solvent accessible surface area (3115 Å^2) than the major conformation (3302 Å^2) (Figure 6B). Additionally, the minor conformation interacts with D145 at the N-terminus of helix δC (Figure 6A,B). Interestingly, compound BDOIA383 in complex with CBP BRD revealed a rotation of the isoxazole-benzimidazole bond by 180°, exposing the phenethyl group to substituted R1173 at the δC N-terminus[46] (PDB ID 5CGP), occupying the space of the *qFit-ligand* minor morpholine conformation in BRD4. Subsequent ligand modifications

DOI: 10.1021/acs.jmedchem.8b01292
J. Med. Chem. XXXX, XXX, XXX−XXX

strengthened these interactions, leading to increasingly selective CBP modulators.

Flipped binding modes between BRD4 and CBP had been observed earlier with a bound isoxazolyl-benzimidazole ligand, also leading to improved selectivity.[47] Strikingly, in this case too, *qFit-ligand* identified a minor conformation in the CBP complex structurally close to the BRD4 bound conformation (Figure 6C). Because selectivity is often achieved by leveraging unique structural ligand−receptor interactions, identifying alternate ligand conformations may help profile auspicious ligand−receptor secondary molecular recognition sites.

Application of *qFit-ligand* to all 126 BRD2−4 crystal structures in the PDB (deposited in Zenodo; DOI: 10.5281/zenodo.1256262) suggests that differential binding modes and ligand heterogeneity are remarkably ubiquitous (Materials and Methods). Visual inspection and manual curation revealed 12 new binding conformations detected with high confidence (Supporting Information, Figure S12) and an additional 24 with possible alternate conformations (Supporting Information, Table S5, Figure S13). The alternate conformation detected by *qFit-ligand* in the crystal structure of BRD4 with ligand 9BM[48] (phenyl ring flip) is the same conformation observed in the crystal structure of BRD2 with ligand S5B,[49] further supporting the idea that ligands can sample a second, minor pose which becomes dominant after small chemical modifications to their structure. These observations and the pervasiveness of ligand heterogeneity in BRDs suggest that the potential of alternate ligand conformations for structure-based drug design is significantly undervalued.

DISCUSSION

Ligand conformational heterogeneity is widespread in X-ray data deposited in the PDB but underreported in the absence of automated and reliable computational methods. *qFit-ligand* is a new method to model a parsimonious multiconformer ligand in crystallographic electron densities. We formulated the challenge of identifying an ensemble that collectively best agrees with the electron density, from up to tens of thousands of candidate conformations, as a stepwise combinatorial optimization problem. *qFit-ligand* relies on exhaustive sampling, iteratively restrained by the electron density, to fully cover the conformational space of each ligand. Our method was designed to provide a measure of statistical confidence for model selection in cases of ligand conformational heterogeneity, separating the contributions between harmonic displacement and multiple conformations.

We highlighted three examples of previously unmodeled alternate ligand conformations obtained from prospective application of *qFit-ligand* to the D3R and *Twilight* data sets (Supporting Information, Table S4 lists all prospective discoveries). Strikingly, even the highly curated D3R data set revealed a previously unmodeled alternate conformation. Targeted application to a single bromodomain receptor suggests that as many as 29% of receptor−ligand crystal structures could have alternate ligand conformations. This is a likely conservative estimate of the accessible ligand conformational landscape in protein crystal structures. The portrait of rigid receptors and ligands is exacerbated by the common practice of collecting X-ray crystallographic data at cryogenic temperature (100 K). Although cryocooling increases the precision of structure determination by reducing thermal motions, cooling affects the conformational distribution of more than 35% of side chains in proteins[50] and has been found to alter ligand binding and abolish transient binding sites observed at room temperature.[51] Applying *qFit-ligand* to room temperature X-ray crystallography data, which can shift the equilibrium of receptor−ligand conformational ensembles, may reveal additional minor ligand binding poses that are typically masked in cryogenic data.

qFit-ligand conformational strain energies after refinement were nearly indistinguishable from those of the manually curated benchmark set, signifying that its multiconformer models are chemically accurate. Our analysis showed that *qFit-ligand* conformations were nearly isoenergetic. Less often we identified a ligand for which the *qFit-ligand* multiconformer model significantly reduced strain energy, suggesting that conformational averaging of the single conformer model had led to a poorly modeled ligand to fit the density. Changes in the free energy of the ligand−receptor complex will give a more complete picture of the effect of multiconformer ligands but require a model of the receptor response to binding, which is beyond the scope of the current study. Ironically, multiconformer ligands are commonly filtered out of major test sets for development of docking and conformational sampling approaches but may be a more "trustworthy" representation of the underlying data.[52] Multiconformer ligand models can therefore address important challenges in ligand validation and deposition in the Protein Data Bank (PDB).[53,54]

Several aspects of *qFit-ligand* could be improved in the future. First and foremost, modeling the *joint* conformational ensemble of the binding site residues and ligand will be a major step forward toward a better understanding of receptor response to ligand binding. The potential of this approach is underlined by our finding that 12% of structures in the *Twilight* data set already present alternate receptor conformations within 5 Å of the ligand. While ultimately an accurate thermodynamic distribution for receptor−ligand conformations is desired, our approach determines a parsimonious ensemble of conformations that is supported by the data alone. These conformations can provide a starting point for MD simulation to obtain a better estimation for a thermodynamic distribution. Second, while in principle our conformational sampling approach could be combined with a sophisticated force field,[55] relying on energy restraints in the discovery stage can result in increased computational cost and can risk excluding promising candidate conformations owing to imperfect sampling and steep potential energy gradients. Rather, we advocate including energy restraints in refinement.[31] Other conformational search methods with force fields, such as Schrodinger's ConfGen[56] and MacroModel,[57] OpenEye's Omega,[58] MOE,[59] and many other freely available tools,[60] could independently validate results in the absence of data.

Third, the false-positive rates can likely be decreased. Several techniques are available to guard against overfitting. For example, the BIC criteria weighs increased model complexity (number of conformations) to a better statistical fit. Terminal ends and ring flips had low false positive rates, whereas those for the branched and displaced categories were elevated. *qFit-ligand* recovered terminal end and ring flips to within an nRMSD of 0.27. Disordered parts of branched ligands were often solvent-exposed and therefore more difficult to recover. Accounting for partial occupancy of ligand, receptor conformers, and solvent will be required to reveal details at the solvent interface. Displaced ligands are not "anchored" in the binding pocket and are among the most challenging to recover.

DOI: 10.1021/acs.jmedchem.8b01292
J. Med. Chem. XXXX, XXX, XXX−XXX

An nRMSD of 0.5 or below often sufficed for further refinement, but even nRMSDs up to 0.75 sometimes required only minor manual adjustments, depending on the absolute RMSD between states. For example, ring flips involving rotationally symmetric atom species cannot be uniquely assigned based on the electron density alone, leading to inflated RMSD measures, which are easily adjusted (Supporting Information, Materials and Methods, PDB 3P4V). All benchmark *qFit-ligand* results were obtained with the same parameters. In practice, specific problems will dictate tailored settings. For example, selecting finer sampling steps or larger volumes for rigid body searches could give better results at the expense of increased computational time (Supporting Information, Figure S17). Nonetheless, on our benchmark set, the fully automated *qFit-ligand* multiconformer models were supported by real-space validation measures, and their R_{free} values were statistically indistinguishable from the manually curated set. While these measures cannot perfectly distinguish false positives, structural models consistent with the reflection data create a pool of testable hypothesis, which can be evaluated in drug discovery using ligand structure activity relationships or protein residue mutations.

Fourth, the partial occupancy of an "unbound"/apo state could be explicitly considered. Weak, overlapping densities originating from partially occupied receptor and ligand conformations in the binding pocket are often difficult to tease apart, owing to a vast number of possible ligand conformations to be evaluated, even in sterically constrained binding cavities. Partially occupied water molecules and crystallographic additives often further confound modeling efforts. In these challenging cases, difference densities from alternate states are often incorrectly resolved by waters. Promising new approaches such as PanDDa[61] can reveal the electron density of partially occupied states; however, it requires a large number of "ground state" crystal structures to reliably compute their contribution to the partially occupied state. Our method is highly complementary, and PanDDa maps could even be used as input to *qFit-ligand*. Synergy of these approaches holds the promise to enable efficient, accurate, and unbiased discovery of alternate fragment and ligand binding poses. This is increasingly important in view of the ability to structurally screen hundreds of candidate ligands within hours on modern synchrotrons. The combination of these methods may help remove temptation to fill all difference density with waters while avoiding the overly optimiztic modeling of partial occupancy ligands that are highlighted by the *Twilight Database*.

Even with these improvements, it is important to be sensitive to concerns of overfitting when fitting additional conformations into electron density maps. We have guarded against this possibility in multiple ways: (1) we identify conformations similar to "expert" manual modeling in experimental test sets, (2) in synthetic data sets, the Fisher z score identifies a statistically significant parsimonious set that correspond in number to the underlying "true" number of conformations, and (3) traditional global metrics (R_{free}) and new local metrics (EDIA) do not identify major concerns. Furthermore, on the prospective set (1), new interactions are identified that make biochemical sense, (2) we identified similar conformations in ligands that differ by only a few atoms, and (3) visual inspection confirms that $F_o - F_c$ difference density is reduced. This last point underscores how visual inspection is important for eliminating false positives and, as shown here, for manually improving the fit. Furthermore, these checks are especially important for verifying the correct stereochemistry. Ultimately, biochemical tests with mutations or altered ligands are the best forward validation.

Finally, as the particle size and resolution limitations of single-particle cryoelectron microscopy (cryo-EM) continue to improve, that technology will have a major impact on drug discovery.[62] High-throughput and automation approaches,[63] combined with the size of the complexes in cryo-EM structure determination, will soon turn careful modeling of protein and ligand structural heterogeneity into a major bottleneck. *qFit-ligand* can provide an efficient, automated modeling approach at the amino acid length scale, as EM maps are immutable during modeling and refinement. Beyond applications to drug discovery, as time-resolved serial crystallography is rapidly becoming routine at X-ray free electron lasers and even synchrotrons,[64] *qFit-ligand* can help resolve minor populations of structural protein−ligand intermediates in light-driven pump−probe[65] or structural enzymology "mix-and-inject" experiments.[66,67]

CONCLUSIONS

Revealing the full receptor−ligand conformational ensemble can help drug design by exploiting the balance between entropy and enthalpy in compound design[68,69] and by characterizing the effect of prerigidifying ligands on affinity.[70] Equally important, it can help the rational design of ligand selectivity by exposing accessible molecular surfaces unique to their intended targets.[71] In the future, full integration of *qFit-ligand* with *qFit* could reveal the structural reorganization of binding pockets and allosteric signal propagation in the receptor upon ligand binding.[21,72] Our *qFit-ligand* open source software, available from https://github.com/ExcitedStates/qfit_ligand, provides promising, new starting points for ligand optimization and structure-based drug discovery. However, communication between structural biologists, computational chemists, and medicinal chemists remains a requisite for successful, rational design.

MATERIALS AND METHODS

Survey of the Protein Data Bank and benchmark creation. All structure coordinate files were downloaded from the PDB. Structures determined by X-ray crystallography were checked for *HETATM* entries (ligands) containing at least two different *altloc* identifiers with identical chemical composition. We aim to characterize conformational heterogeneity of ligands that are (1) drug-like and (2) have multiple internal degrees of freedom. Ligands with fewer than 15 non-hydrogen atoms were therefore discarded as were covalently linked ligands. This resulted in a list of 2611 ligands divided over 1845 PDB files. The list was further pruned to exclude ligand flips, i.e., alternate conformations that do not have a common cluster of atoms in space, and alternate conformations consisting exclusively of ring puckers as our algorithm was not designed to sample these types of conformational changes. We then selected receptors and ligands of pharmaceutical interest, resulting in a final benchmark set of 90 cases that refined against the deposited structure factors and CIF files. As the quality of X-ray data affects model building and refinement, we verified that low-resolution X-ray data cutoff and data completeness were within acceptable ranges (Supporting Information, Table S1). Each case was rerefined using phenix.refine v1.11 with the following parameters

For PDBs Better than 1.5 Å. optimize_ xyz_ weight = true optimize_ adp_ weight = true optimize_ mask=True main.number_

DOI: 10.1021/acs.jmedchem.8b01292
J. Med. Chem. XXXX, XXX, XXX−XXX

of_ macro_ cycles=10 adp.individual.anisotropic='not water and not element H' adp.individual.isotropic="water or element H"

For PDBs Worse than 1.5 Å. optimize_ xyz_ weight=true optimize_ adp_ weight=true optimize_ mask=True main.number_ of_ macro_ cycles=10 adp.individual.isotropic=all

Single conformer ligand models were created by removing the ligand's "B" conformation from the original deposited PDB model and resetting the occupancy of the "A" conformation to 1. The single conformer models were re-refined as above.

The *qFit-ligand* Approach. The *qFit-ligand* algorithm takes as input the initial structure of a refined single conformer ligand modeled in the electron density, a real-space map ($2mF_o - DF_c$) in *ccp4* format and its resolution and, optionally, the receptor and other ligand and solvent atoms for clash avoidance. The *qFit-ligand* algorithm starts by scaling the map electron density values to approximate absolute scale, using only the density under the footprint of the receptor. Next, the algorithm calculates an F_c map corresponding to the receptor and any other atoms in the crystal not part of the ligand. This map is subtracted from the experimental density. Map values below the mean are set to zero to prevent building into spurious density. We call the resulting map the *target map*.

Next, *qFit-ligand* determines rotatable covalent bonds of the ligand and rigid groups of atoms. Covalent bonds are determined based on proximity; i.e., if the distance between two atoms is smaller than their combined covalent radius plus 0.5 Å, the atoms are considered covalently bonded. It partitions the ligand into rigid groups of atoms (i.e., groups of atoms without internal DoFs) as follows: It constructs a graph $G = (V_m, E_m)$ such that the vertices V_m represent atoms, and edges E_m represent covalent bonds. Next, members of E_m that (1) are in a ring system, and (2) edges (u,v) in E_m where u or v has degree one are edge-contracted. Hybridization states (partial double bonds) are ignored in the current implementation. A covalent bond is rotatable if it is not part of the same ring system. After edge contraction, each edge E_m ultimately corresponds to a rotating bond (one degree of freedom) and each vertex V_m corresponds to a collection of atoms that form a rigid body. Thus, rigid groups of atoms do not have internal, rotatable covalent bonds (Supporting Information, Figure S2).

Analogous to existing crystallographic model building procedures,[73] *qFit-ligand* iteratively generates and ranks a large number of candidate ensembles by scoring against the electron density and retaining a small ensemble (Figure 3A and Supporting Information, Figure S2). It uses modern statistical routines for subset selection in regression models by MIQP.[74,75] *qFit-ligand* builds up candidate ligand conformers starting from each rigid group of atoms in turn, similar to the approach implemented in FlexX/S[76] (Supporting Information, Figure S2). To prevent a combinatorial explosion, *qFit-ligand* iteratively samples and selects candidate conformers for successive rigid groups. The first sampling iteration consists of a local rigid body search of the starting group within a box with an edge size of 0.4 Å at a 0.1 Å interval and 10 randomly generated orientations at a maximum rotation angle of 10° (1250 conformations). An MIQP step (details below) selects up to five occupancy-weighted candidate positions that, collectively, minimize the real-space density residual of the rigid group. For each selected conformation, subsequent iterations each sample N (user-defined, default 2) torsion angles with a user-defined (default 6°) step size to add N successive rigid groups simultaneously. Clash detection is divided into internal clashes, i.e., clashes within a single ligand conformer, and external clashes, i.e., clashes between a ligand conformer and the receptor. Clashing conformations, both internal and with the receptor (using an efficient, $\mathbf{O}(1)$, spatial hashing algorithm), are detected and removed from the set before selection with MIQP. Bond lengths and angles are kept fixed during the whole procedure.

After each sampling iteration, the optimal occupancies of generated conformations are determined as follows. Each conformation is transformed into a density given by

$$\rho(r) = 8/r \int_{s_{\min}}^{s_{\max}} f(s)\, \exp(-Bs^2)\, \sin(4\pi rs)s\, ds$$

where r is the position compared to the atom position, $f(s)$ is the atomic scattering factor as a function of the momentum vector of the atom, B is the isotropic B-factor, and $s_{\min}$ and $s_{\max}$ are the minimum and maximum momentum vector length. For computational efficiency, a lookup table is created for each atom at an interval of 0.01 Å.

A combined mask is calculated by forming the union of all individual conformation masks, using a resolution dependent radius, where $r = 0.5 + R/3$. Density values under the footprint of the resulting mask are extracted and used as input for Quadratic Programming (QP) and Mixed Integer Quadratic Programming (MIQP) to select up to five conformations that best represent the density data locally. QP and MIQP solvers guarantee the global optimal occupancy of each conformation by minimizing the real-space residual given by

$$\begin{aligned} &\min_{w} \|\rho^o - \textstyle\sum_i w_i \rho_i^c\|_2 \\ &\text{s.t.} \quad w_i \geq t_{d_{\min}}, \ i = 1, \ldots, n \\ &\qquad 0 \leq \textstyle\sum_i w_i \leq 1 \end{aligned} \tag{1}$$

where ρ^o is the target map, ρ_i is the calculated density of conformer i, w_i is the weight, or occupancy, of conformer i, and $0 \leq t \leq 1$ is a threshold on the occupancy. If $t = 0$, the constraints enforce non-negativity for the occupancies, and the program is a QP. The combined occupancy cannot exceed unity. Selecting $t > 0$ introduces sparsity or threshold constraints, which turns the program (1) into a MIQP. To reduce computational complexity, relevant conformations are preselected using QP and used as input for a subsequent round of MIQP.[23]

After the ligand has been fully built up starting from each cluster, all resulting conformations are pooled together for a final round of rescoring. The individual Pearson product-moment cross-correlation (RSCC) is calculated for each individual conformation. Conformations with RSCC score less than 0.9 times the highest correlation, and redundant conformations for which all pairwise atom distances are within those of previously accepted conformations, are discarded. Finally, a parsimonious multiconformer model is created as follows. An MIQP step at an occupancy threshold of 0.20 is performed on the remaining pool of conformations. Visual inspection of conformers at minimum occupancy of 0.2 generally indicated density contours exceeded noise levels.[77] For very high resolution data sets, this threshold can be reduced. The resulting selected conformations are ranked by RSCC value, and starting from the conformation carrying the highest RSCC, additional conformations are added if the RSCC increases under the combined footprint and else discarded. This is performed iteratively until self-consistent, i.e., all conformations increase the RSCC under the combined footprint. The output of *qFit-ligand* consists of all conformations before the final rescoring round and the sparse, occupancy-weighted multiconformer ligand model.

qFit-ligand is implemented in Python 2.7 and relies on the open-source NumPy, SciPy, and CVXOPT[78] packages and the freely available Community Edition of IBM ILOG CPLEX, with added modules from the mmLib Python toolkit.[79] *qFit-ligand* is released under the MIT license and can be downloaded free of charge from https://github.com/ExcitedStates/qfit_ligand, where additional documentation and installation instructions can be found.

Benchmarking *qFit-ligand*. Simulated structure factors were generated from the rerefined benchmark set using *phenix.fmodel* at 1.0, 1.3, 1.6, 2.0, and 2.5 Å resolution. Occupancy of the B-conformer was varied from 0.5 to 0.0 occupancy in 0.1 decrements, requiring that the combined occupancy of the multiconformer ligand summed up to unity. A random error of 10% was added to the amplitudes, a fraction of 0.1 was used for R_{free} flags, and we selected $k_{sol} = 0.4$ and $b_{sol} = 45$ Å^2. The B-factor of each ligand atom was adjusted by 10 times the difference in real and simulated resolution, i.e., the B-factor was inflated for lower resolution simulated data and sharpened for high resolution data. The resulting *mtz* files were converted into *ccp4* density files using *phenix.mtz2map*.

DOI: 10.1021/acs.jmedchem.8b01292
J. Med. Chem. XXXX, XXX, XXX−XXX

For each resolution and occupancy combination, *qFit-ligand* was run on the full benchmark set using different sampling parameters: sampling 1 degree of freedom (DoF) using a torsion sampling interval of 1 degree, and sampling 2 DoFs simultaneously using a torsion sampling interval of 6 degrees. To obtain a uniform metric for evaluating the performance of *qFit-ligand*, we therefore analyzed the results by calculating a normalized RMSD, calculated in the receptor frame of reference:[80,81]

$$\mathrm{nRMSD} = \min C_i \frac{\mathrm{RMSD}(B, C_i)}{\mathrm{RMSD}(A, B)}$$

between the output structures C_i of *qFit-ligand* and the ligand B conformer used during the structure factor generation, normalized by the RMSD between the A and B conformer. Conformers C_i for which nRMSD < 0.5 are more similar to the B conformer than the A conformer. The nRMSD measure puts equal weight on each benchmark case by normalization while providing uniform thresholds for determining success (Figure S14). We note that the RMSD (and therefore also the nRMSD) measure has important limitations, affecting the results. For example, because RMSD is typically calculated between unique points, it fails to account for symmetric transformations within a ligand, e.g., a 180° flipped acidic group or aromatic ring, thus introducing additional error. Unfortunately, to our knowledge, there is no readily available method that addresses this issue. While a low nRMSD guarantees a good solution, a relatively high nRMSD can still suggest an alternate conformation that requires some manual adjustments, including symmetric transformations.

We subsequently evaluated the performance of *qFit-ligand* for each category in the benchmark set, at simulated resolutions and occupancies, after refinement with PHENIX v1.11 using the same protocol as stated above for rerefinement. The final selection stage was optimized heuristically by finding a balance between maximizing sensitivity and minimizing false-positives against the benchmark.

D3R and *Twilight Database* Investigation. We downloaded the D3R (https://drugdesigndata.org/about/datasets) and Twilight (http://www.ruppweb.org/twilight/newligands-2016.tsv.bz2) databases deposited in 2016. For all cases, structure coordinates and $2mF_o - DF_c$ maps were downloaded from the PDB. For the *Twilight* cases, we discarded structures with a reported resolution worse than 2.0 Å and ligands consisting of less than 15 and more than 35 non-hydrogen atoms and a cross-correlation score less than 0.6. The resulting *qFit-ligand* multiconformer models were ranked on the Fisher z-transformation score. The Fisher z-transformation is a mapping of the RSCC r so that its distribution is approximately normal. It was previously applied to significance testing for cryo-EM rigid body fitting[82−84] and is given by

$$z = \frac{1}{2}\ln\left(\frac{1+r}{1-r}\right)$$

where r is the RSCC. The standard error of z is given by

$$\sigma = \frac{1}{\sqrt{N-3}}$$

where N represents the number of independent observations, approximated by $N = MV/(c \times R)$, where MV represents the molecular volume of the ligand in Å^3, R the resolution in Å, and $c = 1$ Å^2, a constant.[83] Starting with the conformer with the highest RSCC, additional conformations are added. Our approach is based on hypothesis testing of the normally distributed, random variable. For each additional conformer, the z-score is recalculated for both the starting conformation and the combined multiconformer under the footprint of the latter. The resulting difference in z-score is divided by its standard error to provide a resolution and size corrected measure of significance for the increase in cross-correlation, where higher is better. The test statistic is

$$\xi_i = \frac{z_i^{\Sigma} - z_{\mathrm{best}}}{\sigma_z}$$

where Z_{best} is the recalculated z-score of the single conformer with the highest RSCC, and z^{Σ}_i is the z-score of the ith combined multiconformer. The highest z-score increase found during this iterative process is reported in Supporting Information, Table S3.

EDIAm and OPIA Calculation.

$$\mathrm{EDIA}_m(U) = \sum_{U_x \in U} \left(\mathrm{occ}(U_x) \times \left[\left(\frac{1}{|U_x|} \sum_{a \in Ux} (\mathrm{EDIA}(a) - 0.1)^{-1/2} \right)^{-2} + 0.1 \right] \right)$$

where U_x is a conformer of the ligand U, a is an atom in U_x with an EDIA score of EDIA(a), and occ(U_x) is the occupancy of that conformer. The OPIA of multiconformer mode was calculated as an occupancy-weighted average of the OPIA of each conformer.

Ligand Energy. To assess ligand conformational energies, we carried out constrained minimizations (flat bottom width of 0.2 Å) of all ligands (from single conformer and *qFit-ligand* multiconformer models) using Jaguar[85] with the M06-2X functional[86,87] and 6-31G(d,p) basis set, except for bromine atoms, which used the LAV2P basis set. Gas-phase energies of ligand conformations generated by *qFit-ligand* (which were subsequently refined) were compared to ligand conformations in the single conformer model (i.e., 0 kcal/mol). The relative energies of each alternative conformation in the *qFit-ligand* multiconformer model were multiplied by their respective occupancies, then summed to arrive at the occupancy-weighted ligand energy.

■ ASSOCIATED CONTENT

Supporting Information

The Supporting Information is available free of charge on the ACS Publications website at DOI: 10.1021/acs.jmedchem.8b01292.

Additional statistics for our data sets and results, detailed flowchart of the *qFit-ligand* algorithm, and molecular visualizations of its multiconformer models (PDF)

Overview of benchmark cases and categorization of conformational change between alternate conformers (PDF)

Performance of *qFit-ligand* on the benchmark using re-refined deposited data, showing quality metrics of re-refined single conformer structures, re-refined multiconformer deposited structures, and refined *qfit-ligand* generated structures (PDF)

Results of applying *qFit-ligand* on a subset of the *Twilight Database* (PDF)

Overview of prospective cases with an unmodeled alternate conformer found by *qFit-ligand* (PDF)

BRD4 structures subjected to *qFit-ligand* approach, ordered by the Fisher z-score (PDF)

Accession Codes

6DMG (remodeled 4FV3); 6DMH (remodeled 4EV4); 6DMI (remodeled 5EZX); 6DMJ (remodeled 5CFW); 6DMK (remodeled 4NR5); 6DML (remodeled 4BW3).

■ AUTHOR INFORMATION

Corresponding Author

*E-mail: vdbedem@stanford.edu. Phone: +1 (650) 776-5365.

ORCID

Brandi M. Hudson: 0000-0003-2288-9157

Henry van den Bedem: 0000-0003-2358-841X

DOI: 10.1021/acs.jmedchem.8b01292
J. Med. Chem. XXXX, XXX, XXX−XXX

Present Address

[#]D.A.K.: CUNY Advanced Science Research Center Department of Chemistry and Biochemistry, City College of New York

Author Contributions

G.C.P.v.Z. and B.M.H. contributed equally. G.C.P.v.Z., R.F., A.H., and H.v.d.B. developed and implemented core algorithms; G.C.P.v.Z., B.M.H., S.H.P.d.O., K.B., T.D., J.S.F., and H.v.d.B. analyzed data; D.A.K. and P.S. contributed code and data analysis. J.S.F. and H.v.d.B. conceived the study. G.C.P.v.Z., B.M.H., J.S.F., and H.v.d.B. wrote the manuscript. All authors edited the manuscript.

Notes

The authors declare the following competing financial interest(s): J.S.F. is a paid consultant and has a financial stake in Relay Therapeutics. G.C.P.v.Z., K.B., and T.D. are employees of Schrödinger.

■ ACKNOWLEDGMENTS

We gratefully acknowledge support from Relay Therapeutics. D.A.K. was supported by an A.P. Giannini Postdoctoral Fellowship. R.F. is supported by a Novo Nordisk Foundation and Stanford Bio-X Program fellowship NNF15OC0015268. J.S.F. is supported by a Searle Scholar Award from the Kinship Foundation, a Pew Scholar Award from the Pew Charitable Trusts, a Packard Fellowship from the David and Lucile Packard Foundation, NIH GM124149, UC Office of the President Laboratory Fees Research Program LFR-17-476732, and NSF STC-1231306. S.H.P.d.O., J.S.F., and H.v.d.B. are supported by NIH GM123159.

■ ABBREVIATIONS USED

BRD4, bromodomain-containing protein 4; CBP, CREB binding protein; D3R, Drug Design Data Resource; EDIAm, Electron Density Support for Individual Atoms; RSCC, Pearson product-moment cross-correlation

■ REFERENCES

(1) Tzeng, S.-R.; Kalodimos, C. G. Protein Activity Regulation by Conformational Entropy. *Nature* **2012**, *488*, 236−240.

(2) Caro, J. A.; Harpole, K. W.; Kasinath, V.; Lim, J.; Granja, J.; Valentine, K. G.; Sharp, K. A.; Wand, A. J. Entropy in Molecular Recognition by Proteins. *Proc. Natl. Acad. Sci. U. S. A.* **2017**, *114* (25), 6563−6568.

(3) Mobley, D. L.; Dill, K. A. Binding of Small-Molecule Ligands to Proteins: "What You See" Is Not Always "What You Get. *Structure* **2009**, *17* (4), 489−498.

(4) van den Bedem, H.; Fraser, J. S. Integrative, Dynamic Structural Biology at Atomic Resolution—it's about Time. *Nat. Methods* **2015**, *12* (4), 307−318.

(5) Smith, J. L.; Hendrickson, W. A.; Honzatko, R. B.; Sheriff, S. Structural Heterogeneity in Protein Crystals. *Biochemistry* **1986**, *25* (18), 5018−5027.

(6) Lang, P. T.; Ng, H.-L.; Fraser, J. S.; Corn, J. E.; Echols, N.; Sales, M.; Holton, J. M.; Alber, T. Automated Electron-Density Sampling Reveals Widespread Conformational Polymorphism in Proteins. *Protein Sci.* **2010**, *19* (7), 1420−1431.

(7) Burnley, B. T.; Afonine, P. V.; Adams, P. D.; Gros, P. Modelling Dynamics in Protein Crystal Structures by Ensemble Refinement. *eLife* **2012**, *1*, e00311.

(8) Carroll, M. J.; Mauldin, R. V.; Gromova, A. V.; Singleton, S. F.; Collins, E. J.; Lee, A. L. Evidence for Dynamics in Proteins as a Mechanism for Ligand Dissociation. *Nat. Chem. Biol.* **2012**, *8* (3), 246−252.

(9) Carroll, M. J.; Gromova, A. V.; Miller, K. R.; Tang, H.; Wang, X. S.; Tripathy, A.; Singleton, S. F.; Collins, E. J.; Lee, A. L. Direct Detection of Structurally Resolved Dynamics in a Multiconformation Receptor-Ligand Complex. *J. Am. Chem. Soc.* **2011**, *133* (16), 6422−6428.

(10) Martinek, T. A.; Otvös, F.; Dervarics, M.; Tóth, G.; Fülöp, F. Ligand-Based Prediction of Active Conformation by 3D-QSAR Flexibility Descriptors and Their Application in 3 + 3D-QSAR Models. *J. Med. Chem.* **2005**, *48*, 3239−3250.

(11) Kuhnert, M.; Köster, H.; Bartholomäus, R.; Park, A. Y.; Shahim, A.; Heine, A.; Steuber, H.; Klebe, G.; Diederich, W. E. Tracing Binding Modes in Hit-to-Lead Optimization: Chameleon-like Poses of Aspartic Protease Inhibitors. *Angew. Chem., Int. Ed.* **2015**, *54* (9), 2849−2853.

(12) Kozakov, D.; Hall, D. R.; Jehle, S.; Luo, L.; Ochiana, S. O.; Jones, E. V.; Pollastri, M.; Allen, K. N.; Whitty, A.; Vajda, S. Ligand Deconstruction: Why Some Fragment Binding Positions Are Conserved and Others Are Not. *Proc. Natl. Acad. Sci. U. S. A.* **2015**, *112*, E2585−E2594.

(13) Han, X.; Jiang, M.; Zhou, C.; Zhou, Z.; Xu, Z.; Wang, L.; Mayweg, A. V.; Niu, R.; Jin, T.-G.; Yang, S. Discovery of Potent and Selective CDK8 Inhibitors through FBDD Approach. *Bioorg. Med. Chem. Lett.* **2017**, *27* (18), 4488−4492.

(14) Casale, E.; Amboldi, N.; Brasca, M. G.; Caronni, D.; Colombo, N.; Dalvit, C.; Felder, E. R.; Fogliatto, G.; Galvani, A.; Isacchi, A.; Polucci, P.; Riceputi, L.; Sola, F.; Visco, C.; Zuccotto, F.; Casuscelli, F. Fragment-Based Hit Discovery and Structure-Based Optimization of Aminotriazoloquinazolines as Novel Hsp90 Inhibitors. *Bioorg. Med. Chem.* **2014**, *22* (15), 4135−4150.

(15) Mpamhanga, C. P.; Spinks, D.; Tulloch, L. B.; Shanks, E. J.; Robinson, D. A.; Collie, I. T.; Fairlamb, A. H.; Wyatt, P. G.; Frearson, J. A.; Hunter, W. N.; Gilbert, I. H.; Brenk, R. One Scaffold, Three Binding Modes: Novel and Selective Pteridine Reductase 1 Inhibitors Derived from Fragment Hits Discovered by Virtual Screening. *J. Med. Chem.* **2009**, *52* (14), 4454−4465.

(16) Woolford, A. J.-A.; Pero, J. E.; Aravapalli, S.; Berdini, V.; Coyle, J. E.; Day, P. J.; Dodson, A. M.; Grondin, P.; Holding, F. P.; Lee, L. Y.W.; Li, P.; Manas, E. S.; Marino, J., Jr; Martin, A. C.L.; McCleland, B. W.; McMenamin, R. L.; Murray, C. W.; Neipp, C. E.; Page, L. W.; Patel, V. K.; Potvain, F.; Rich, S.; Rivero, R. A.; Smith, K.; Somers, D. O.; Trottet, L.; Velagaleti, R.; Williams, G.; Xie, R. Exploitation of a Novel Binding Pocket in Human Lipoprotein-Associated Phospholipase A2 (Lp-PLA2) Discovered through X-Ray Fragment Screening. *J. Med. Chem.* **2016**, *59* (11), 5356−5367.

(17) Plattner, N.; Noé, F. Protein Conformational Plasticity and Complex Ligand-Binding Kinetics Explored by Atomistic Simulations and Markov Models. *Nat. Commun.* **2015**, *6*, 7653.

(18) Porter, N. J.; Mahendran, A.; Breslow, R.; Christianson, D. W. Unusual Zinc-Binding Mode of HDAC6-Selective Hydroxamate Inhibitors. *Proc. Natl. Acad. Sci. U. S. A.* **2017**, *114* (51), 13459−13464.

(19) Bardelle, C.; Coleman, T.; Cross, D.; Davenport, S.; Kettle, J. G.; Ko, E. J.; Leach, A. G.; Mortlock, A.; Read, J.; Roberts, N. J.; Robins, P.; Williams, E. J. Inhibitors of the Tyrosine Kinase EphB4. Part 2: Structure-Based Discovery and Optimisation of 3,5-Bis Substituted Anilinopyrimidines. *Bioorg. Med. Chem. Lett.* **2008**, *18* (21), 5717−5721.

(20) Lee, C.-J.; Liang, X.; Wu, Q.; Najeeb, J.; Zhao, J.; Gopalaswamy, R.; Titecat, M.; Sebbane, F.; Lemaitre, N.; Toone, E. J.; Zhou, P. Drug Design from the Cryptic Inhibitor Envelope. *Nat. Commun.* **2016**, *7*, 10638.

(21) van den Bedem, H.; Bhabha, G.; Yang, K.; Wright, P. E.; Fraser, J. S. Automated Identification of Functional Dynamic Contact Networks from X-Ray Crystallography. *Nat. Methods* **2013**, *10*, 896−902.

(22) van den Bedem, H.; Dhanik, A.; Latombe, J.-C.; Deacon, A. M. Modeling Discrete Heterogeneity in X-Ray Diffraction Data by Fitting Multi-Conformers. *Acta Crystallogr., Sect. D: Biol. Crystallogr.* **2009**, *65*, 1107−1117.

DOI: 10.1021/acs.jmedchem.8b01292
J. Med. Chem. XXXX, XXX, XXX−XXX

(23) Keedy, D. A.; Fraser, J. S.; van den Bedem, H. Exposing Hidden Alternative Backbone Conformations in X-Ray Crystallography Using qFit. *PLoS Comput. Biol.* **2015**, *11* (10), No. e1004507.
(24) Levin, E. J.; Kondrashov, D. A.; Wesenberg, G. E.; Phillips, G. N., Jr. Ensemble Refinement of Protein Crystal Structures. *Structure* **2007**, *15* (9), 1040−1052.
(25) Diller, D. J.; Pohl, E.; Redinbo, M. R.; Hovey, B. T.; Hol, W. G. A Rapid Method for Positioning Small Flexible Molecules, Nucleic Acids, and Large Protein Fragments in Experimental Electron Density Maps. *Proteins: Struct., Funct., Genet.* **1999**, *36* (4), 512−525.
(26) Oldfield, T. J. X-LIGAND: An Application for the Automated Addition of Flexible Ligands into Electron Density. *Acta Crystallogr., Sect. D: Biol. Crystallogr.* **2001**, *57*, 696−705.
(27) Zwart, P. H.; Langer, G. G.; Lamzin, V. S. Modelling Bound Ligands in Protein Crystal Structures. *Acta Crystallogr., Sect. D: Biol. Crystallogr.* **2004**, *60*, 2230−2239.
(28) Aishima, J.; Russel, D. S.; Guibas, L. J.; Adams, P. D.; Brunger, A. T. Automated Crystallographic Ligand Building Using the Medial Axis Transform of an Electron-Density Isosurface. *Acta Crystallogr., Sect. D: Biol. Crystallogr.* **2005**, *61*, 1354−1363.
(29) Terwilliger, T. C.; Klei, H.; Adams, P. D.; Moriarty, N. W.; Cohn, J. D. Automated Ligand Fitting by Core-Fragment Fitting and Extension into Density. *Acta Crystallogr., Sect. D: Biol. Crystallogr.* **2006**, *62*, 915−922.
(30) Evrard, G. X.; Langer, G. G.; Perrakis, A.; Lamzin, V. S. Assessment of Automatic Ligand Building in ARP/wARP. *Acta Crystallogr., Sect. D: Biol. Crystallogr.* **2007**, *63*, 108−117.
(31) Janowski, P. A.; Moriarty, N. W.; Kelley, B. P.; Case, D. A.; York, D. M.; Adams, P. D.; Warren, G. L. Improved Ligand Geometries in Crystallographic Refinement Using AFITT in PHENIX. *Acta Crystallogr. D Struct Biol.* **2016**, *72*, 1062−1072.
(32) Weichenberger, C. X.; Pozharski, E.; Rupp, B. Visualizing Ligand Molecules in Twilight Electron Density. *Acta Crystallogr., Sect. F: Struct. Biol. Cryst. Commun.* **2013**, *69*, 195−200.
(33) Adams, P. D.; Afonine, P. V.; Bunkóczi, G.; Chen, V. B.; Davis, I. W.; Echols, N.; Headd, J. J.; Hung, L.-W.; Kapral, G. J.; Grosse-Kunstleve, R. W.; McCoy, A. J.; Moriarty, N. W.; Oeffner, R.; Read, R. J.; Richardson, D. C.; Richardson, J. S.; Terwilliger, T. C.; Zwart, P. H. PHENIX: A Comprehensive Python-Based System for Macromolecular Structure Solution. *Acta Crystallogr., Sect. D: Biol. Crystallogr.* **2010**, *66*, 213−221.
(34) Bhat, T. N. Correlation between Occupancy and Temperature Factors of Solvent Molecules in Crystal Structures of Proteins. *Acta Crystallogr., Sect. A: Found. Crystallogr.* **1989**, *45*, 145−146.
(35) Carugo, O. Correlation between Occupancy and B Factor of Water Molecules in Protein Crystal Structures. *Protein Eng., Des. Sel.* **1999**, *12* (12), 1021−1024.
(36) Meyder, A.; Nittinger, E.; Lange, G.; Klein, R.; Rarey, M. Estimating Electron Density Support for Individual Atoms and Molecular Fragments in X-Ray Structures. *J. Chem. Inf. Model.* **2017**, *57* (10), 2437−2447.
(37) Lewis, R. T.; Bode, C. M.; Choquette, D. M.; Potashman, M.; Romero, K.; Stellwagen, J. C.; Teffera, Y.; Moore, E.; Whittington, D. A.; Chen, H.; Epstein, L. F.; Emkey, R.; Andrews, P. S.; Yu, V. L.; Saffran, D. C.; Xu, M.; Drew, A.; Merkel, P.; Szilvassy, S.; Brake, R. L. The Discovery and Optimization of a Novel Class of Potent, Selective, and Orally Bioavailable Anaplastic Lymphoma Kinase (ALK) Inhibitors with Potential Utility for the Treatment of Cancer. *J. Med. Chem.* **2012**, *55* (14), 6523−6540.
(38) Perola, E.; Charifson, P. S. Conformational Analysis of Drug-Like Molecules Bound to Proteins: An Extensive Study of Ligand Reorganization upon Binding. *J. Med. Chem.* **2004**, *47* (10), 2499−2510.
(39) Young, T.; Abel, R.; Kim, B.; Berne, B. J.; Friesner, R. A. Motifs for Molecular Recognition Exploiting Hydrophobic Enclosure in Protein-Ligand Binding. *Proc. Natl. Acad. Sci. U. S. A.* **2007**, *104* (3), 808−813.
(40) Klebe, G. Applying Thermodynamic Profiling in Lead Finding and Optimization. *Nat. Rev. Drug Discovery* **2015**, *14* (2), 95−110.
(41) Howard, J. A.K.; Hoy, V. J.; O'Hagan, D.; Smith, G. T. How Good Is Fluorine as a Hydrogen Bond Acceptor? *Tetrahedron* **1996**, *52* (38), 12613−12622.
(42) Kuhn, B.; Guba, W.; Hert, J.; Banner, D.; Bissantz, C.; Ceccarelli, S.; Haap, W.; Körner, M.; Kuglstatter, A.; Lerner, C.; Mattei, P.; Neidhart, W.; Pinard, E.; Rudolph, M. G.; Schulz-Gasch, T.; Woltering, T.; Stahl, M. A Real-World Perspective on Molecular Design. *J. Med. Chem.* **2016**, *59* (9), 4087−4102.
(43) Filippakopoulos, P.; Picaud, S.; Mangos, M.; Keates, T.; Lambert, J.-P.; Barsyte-Lovejoy, D.; Felletar, I.; Volkmer, R.; Müller, S.; Pawson, T.; Gingras, A.-C.; Arrowsmith, C. H.; Knapp, S. Histone Recognition and Large-Scale Structural Analysis of the Human Bromodomain Family. *Cell* **2012**, *149* (1), 214−231.
(44) Arrowsmith, C. H.; Bountra, C.; Fish, P. V.; Lee, K.; Schapira, M. Epigenetic Protein Families: A New Frontier for Drug Discovery. *Nat. Rev. Drug Discovery* **2012**, *11* (5), 384−400.
(45) Rooney, T. P.C.; Filippakopoulos, P.; Fedorov, O.; Picaud, S.; Cortopassi, W. A.; Hay, D. A.; Martin, S.; Tumber, A.; Rogers, C. M.; Philpott, M.; Wang, M.; Thompson, A. L.; Heightman, T. D.; Pryde, D. C.; Cook, A.; Paton, R. S.; Müller, S.; Knapp, S.; Brennan, P. E.; Conway, S. J. A Series of Potent CREBBP Bromodomain Ligands Reveals an Induced-Fit Pocket Stabilized by a Cation-π Interaction. *Angew. Chem., Int. Ed.* **2014**, *53* (24), 6126−6130.
(46) Chekler, E. L.P.; Pellegrino, J. A.; Lanz, T. A.; Denny, R. A.; Flick, A. C.; Coe, J.; Langille, J.; Basak, A.; Liu, S.; Stock, I. A.; Sahasrabudhe, P.; Bonin, P. D.; Lee, K.; Pletcher, M. T.; Jones, L. H. Transcriptional Profiling of a Selective CREB Binding Protein Bromodomain Inhibitor Highlights Therapeutic Opportunities. *Chem. Biol.* **2015**, *22* (12), 1588−1596.
(47) Hay, D. A.; Fedorov, O.; Martin, S.; Singleton, D. C.; Tallant, C.; Wells, C.; Picaud, S.; Philpott, M.; Monteiro, O. P.; Rogers, C. M.; Conway, S. J.; Rooney, T. P.C.; Tumber, A.; Yapp, C.; Filippakopoulos, P.; Bunnage, M. E.; Müller, S.; Knapp, S.; Schofield, C. J.; Brennan, P. E. Discovery and Optimization of Small-Molecule Ligands for the CBP/p300 Bromodomains. *J. Am. Chem. Soc.* **2014**, *136* (26), 9308−9319.
(48) Mirguet, O.; Lamotte, Y.; Chung, C.-W.; Bamborough, P.; Delannée, D.; Bouillot, A.; Gellibert, F.; Krysa, G.; Lewis, A.; Witherington, J.; Huet, P.; Dudit, Y.; Trottet, L.; Nicodeme, E. Naphthyridines as Novel BET Family Bromodomain Inhibitors. *ChemMedChem* **2014**, *9* (3), 580−589.
(49) Seal, J.; Lamotte, Y.; Donche, F.; Bouillot, A.; Mirguet, O.; Gellibert, F.; Nicodeme, E.; Krysa, G.; Kirilovsky, J.; Beinke, S.; McCleary, S.; Rioja, I.; Bamborough, P.; Chung, C.-W.; Gordon, L.; Lewis, T.; Walker, A. L.; Cutler, L.; Lugo, D.; Wilson, D. M.; Witherington, J.; Lee, K.; Prinjha, R. K. Identification of a Novel Series of BET Family Bromodomain Inhibitors: Binding Mode and Profile of I-BET151 (GSK1210151A). *Bioorg. Med. Chem. Lett.* **2012**, *22* (8), 2968−2972.
(50) Fraser, J. S.; van den Bedem, H.; Samelson, A. J.; Lang, P. T.; Holton, J. M.; Echols, N.; Alber, T. Accessing Protein Conformational Ensembles Using Room-Temperature X-Ray Crystallography. *Proc. Natl. Acad. Sci. U. S. A.* **2011**, *108* (39), 16247−16252.
(51) Fischer, M.; Shoichet, B. K.; Fraser, J. S. One Crystal, Two Temperatures: Cryocooling Penalties Alter Ligand Binding to Transient Protein Sites. *ChemBioChem* **2015**, *16* (11), 1560−1564.
(52) Warren, G. L.; Do, T. D.; Kelley, B. P.; Nicholls, A.; Warren, S. D. Essential Considerations for Using Protein-Ligand Structures in Drug Discovery. *Drug Discovery Today* **2012**, *17* (23−24), 1270−1281.
(53) Adams, P. D.; Aertgeerts, K.; Bauer, C.; Bell, J. A.; Berman, H. M.; Bhat, T. N.; Blaney, J. M.; Bolton, E.; Bricogne, G.; Brown, D.; Burley, S. K.; Case, D. A.; Clark, K. L.; Darden, T.; Emsley, P.; Feher, V. A.; Feng, Z.; Groom, C. R.; Harris, S. F.; Hendle, J.; Holder, T.; Joachimiak, A.; Kleywegt, G. J.; Krojer, T.; Marcotrigiano, J.; Mark, A. E.; Markley, J. L.; Miller, M.; Minor, W.; Montelione, G. T.; Murshudov, G.; Nakagawa, A.; Nakamura, H.; Nicholls, A.; Nicklaus, M.; Nolte, R. T.; Padyana, A. K.; Peishoff, C. E.; Pieniazek, S.; Read, R. J.; Shao, C.; Sheriff, S.; Smart, O.; Soisson, S.; Spurlino, J.; Stouch,

DOI: 10.1021/acs.jmedchem.8b01292
J. Med. Chem. XXXX, XXX, XXX−XXX

T.; Svobodova, R.; Tempel, W.; Terwilliger, T. C.; Tronrud, D.; Velankar, S.; Ward, S. C.; Warren, G. L.; Westbrook, J. D.; Williams, P.; Yang, H.; Young, J. Outcome of the First wwPDB/CCDC/D3R Ligand Validation Workshop. *Structure* **2016**, *24* (4), 502−508.
(54) Berman, H. M.; Westbrook, J.; Feng, Z.; Gilliland, G.; Bhat, T. N.; Weissig, H.; Shindyalov, I. N.; Bourne, P. E. The Protein Data Bank. *Nucleic Acids Res.* **2000**, *28*, 235−242.
(55) Harder, E.; Damm, W.; Maple, J.; Wu, C.; Reboul, M.; Xiang, J. Y.; Wang, L.; Lupyan, D.; Dahlgren, M. K.; Knight, J. L.; Kaus, J. W.; Cerutti, D. S.; Krilov, G.; Jorgensen, W. L.; Abel, R.; Friesner, R. A. OPLS3: A Force Field Providing Broad Coverage of Drug-like Small Molecules and Proteins. *J. Chem. Theory Comput.* **2016**, *12* (1), 281−296.
(56) Watts, K. S.; Dalal, P.; Murphy, R. B.; Sherman, W.; Friesner, R. A.; Shelley, J. C. ConfGen: A Conformational Search Method for Efficient Generation of Bioactive Conformers. *J. Chem. Inf. Model.* **2010**, *50* (4), 534−546.
(57) Watts, K. S.; Dalal, P.; Tebben, A. J.; Cheney, D. L.; Shelley, J. C. Macrocycle Conformational Sampling with MacroModel. *J. Chem. Inf. Model.* **2014**, *54* (10), 2680−2696.
(58) Hawkins, P. C.D.; Skillman, A. G.; Warren, G. L.; Ellingson, B. A.; Stahl, M. T. Conformer Generation with OMEGA: Algorithm and Validation Using High Quality Structures from the Protein Databank and Cambridge Structural Database. *J. Chem. Inf. Model.* **2010**, *50* (4), 572−584.
(59) Labute, P. LowModeMD−Implicit Low-Mode Velocity Filtering Applied to Conformational Search of Macrocycles and Protein Loops. *J. Chem. Inf. Model.* **2010**, *50* (5), 792−800.
(60) Ebejer, J.-P.; Morris, G. M.; Deane, C. M. Freely Available Conformer Generation Methods: How Good Are They? *J. Chem. Inf. Model.* **2012**, *52* (5), 1146−1158.
(61) Pearce, N. M.; Krojer, T.; Bradley, A. R.; Collins, P.; Nowak, R. P.; Talon, R.; Marsden, B. D.; Kelm, S.; Shi, J.; Deane, C. M.; von Delft, F. A Multi-Crystal Method for Extracting Obscured Crystallographic States from Conventionally Uninterpretable Electron Density. *Nat. Commun.* **2017**, *8*, 15123.
(62) Merk, A.; Bartesaghi, A.; Banerjee, S.; Falconieri, V.; Rao, P.; Davis, M. I.; Pragani, R.; Boxer, M. B.; Earl, L. A.; Milne, J. L.S.; Subramaniam, S. Breaking Cryo-EM Resolution Barriers to Facilitate Drug Discovery. *Cell* **2016**, *165* (7), 1698−1707.
(63) Cheng, A.; Tan, Y. Z.; Dandey, V. P.; Potter, C. S.; Carragher, B. Strategies for Automated CryoEM Data Collection Using Direct Detectors. In *Methods in Enzymology*; Crowther, R. A., Ed.; Academic Press: London, 2016; Vol. *579*, pp 87−102.
(64) Stellato, F.; Oberthür, D.; Liang, M.; Bean, R.; Gati, C.; Yefanov, O.; Barty, A.; Burkhardt, A.; Fischer, P.; Galli, L.; Kirian, R. A.; Meyer, J.; Panneerselvam, S.; Yoon, C. H.; Chervinskii, F.; Speller, E.; White, T. A.; Betzel, C.; Meents, A.; Chapman, H. N. Room-Temperature Macromolecular Serial Crystallography Using Synchrotron Radiation. *IUCrJ* **2014**, *1*, 204−212.
(65) Tenboer, J.; Basu, S.; Zatsepin, N.; Pande, K.; Milathianaki, D.; Frank, M.; Hunter, M.; Boutet, S.; Williams, G. J.; Koglin, J. E.; Oberthuer, D.; Heymann, M.; Kupitz, C.; Conrad, C.; Coe, J.; Roy-Chowdhury, S. U.; Weierstall, U.; James, D.; Wang, D.; Grant, T.; Barty, A.; Yefanov, O.; Scales, J.; Gati, C.; Seuring, C.; Srajer, V.; Henning, R.; Schwander, P.; Fromme, R.; Ourmazd, A.; Moffat, K.; Van Thor, J. J.; Spence, J. C. H.; Fromme, P.; Chapman, H. N.; Schmidt, M. Time-Resolved Serial Crystallography Captures High-Resolution Intermediates of Photoactive Yellow Protein. *Science* **2014**, *346*, 1242−1246.
(66) Kupitz, C.; Olmos, J. L., Jr; Holl, M.; Tremblay, L.; Pande, K.; Pandey, S.; Oberthür, D.; Hunter, M.; Liang, M.; Aquila, A.; Tenboer, J.; Calvey, G.; Katz, A.; Chen, Y.; Wiedorn, M. O.; Knoska, J.; Meents, A.; Majriani, V.; Norwood, T.; Poudyal, I.; Grant, T.; Miller, M. D.; Xu, W.; Tolstikova, A.; Morgan, A.; Metz, M.; Martin-Garcia, J. M.; Zook, J. D.; Roy-Chowdhury, S.; Coe, J.; Nagaratnam, N.; Meza, D.; Fromme, R.; Basu, S.; Frank, M.; White, T.; Barty, A.; Bajt, S.; Yefanov, O.; Chapman, H. N.; Zatsepin, N.; Nelson, G.; Weierstall, U.; Spence, J.; Schwander, P.; Pollack, L.; Fromme, P.; Ourmazd, A.; Phillips, G. N., Jr; Schmidt, M. Structural Enzymology Using X-Ray Free Electron Lasers. *Struct. Dyn.* **2017**, *4* (4), 044003.
(67) Olmos, J.; Pandey, S.; Martin-Garcia, J. M.; Calvey, G.; Katz, A.; Knoska, J.; Kupitz, C.; Hunter, M. S.; Liang, M.; Oberthuer, D.; Yefanov, O.; Wiedorn, M.; Heyman, M.; Holl, M.; Pande, K.; Barty, A.; Miller, M. D.; Stern, S.; Roy-Chowdhury, S.; Coe, J.; Nagaratnam, N.; Zook, J.; Verburgt, J.; Norwood, T.; Poudyal, I.; Xu, D.; Koglin, J.; Seaberg, M. H.; Zhao, Y.; Bajt, S.; Grant, T.; Mariani, V.; Nelson, G.; Subramanian, G.; Bae, E.; Fromme, R.; Fung, R.; Schwander, P.; Frank, M.; White, T. A.; Weierstall, U.; Zatsepin, N.; Spence, J.; Fromme, P.; Chapman, J. N.; Pollack, L.; Tremblay, L.; Ourmazd, A.; Phillips, G. N.; Schmidt, M. Authentic Enzyme Intermediates Captured" on-the-Fly" by Mix-and-Inject Serial Crystallography. *BMC Biol.* **2018**, *16*, 59.
(68) Velazquez-Campoy, A.; Todd, M. J.; Freire, E. HIV-1 Protease Inhibitors: Enthalpic versus Entropic Optimization of the Binding Affinity. *Biochemistry* **2000**, *39* (9), 2201−2207.
(69) Chodera, J. D.; Mobley, D. L. Entropy-Enthalpy Compensation: Role and Ramifications in Biomolecular Ligand Recognition and Design. *Annu. Rev. Biophys.* **2013**, *42*, 121−142.
(70) You, W.; Huang, Y.-M. M.; Kizhake, S.; Natarajan, A.; Chang, C.-E. A. Characterization of Promiscuous Binding of Phosphor Ligands to Breast-Cancer-Gene 1 (BRCA1) C-Terminal (BRCT): Molecular Dynamics, Free Energy, Entropy and Inhibitor Design. *PLoS Comput. Biol.* **2016**, *12* (8), No. e1005057.
(71) Huggins, D. J.; Sherman, W.; Tidor, B. Rational Approaches to Improving Selectivity in Drug Design. *J. Med. Chem.* **2012**, *55* (4), 1424−1444.
(72) Brock, J. S.; Hamberg, M.; Balagunaseelan, N.; Goodman, M.; Morgenstern, R.; Strandback, E.; Samuelsson, B.; Rinaldo-Matthis, A.; Haeggström, J. Z. A Dynamic Asp-Arg Interaction Is Essential for Catalysis in Microsomal Prostaglandin E2 Synthase. *Proc. Natl. Acad. Sci. U. S. A.* **2016**, *113* (4), 972−977.
(73) Terwilliger, T. C. Automated Main-Chain Model Building by Template Matching and Iterative Fragment Extension. *Acta Crystallogr., Sect. D: Biol. Crystallogr.* **2003**, *59*, 38−44.
(74) Bertsimas, D.; Shioda, R. Algorithm for Cardinality-Constrained Quadratic Optimization. *Comput. Optim. Appl.* **2009**, *43* (1), 1−22.
(75) Miyashiro, R.; Takano, Y. Subset Selection by Mallows' Cp: A Mixed Integer Programming Approach. *Expert Syst. Appl.* **2015**, *42* (1), 325−331.
(76) Lemmen, C.; Lengauer, T.; Klebe, G. FLEXS: A Method for Fast Flexible Ligand Superposition. *J. Med. Chem.* **1998**, *41* (23), 4502−4520.
(77) Lang, P. T.; Holton, J. M.; Fraser, J. S.; Alber, T. Protein Structural Ensembles Are Revealed by Redefining X-Ray Electron Density Noise. *Proc. Natl. Acad. Sci. U. S. A.* **2014**, *111* (1), 237−242.
(78) Andersen, M. S.; Dahl, J.; Vandenberghe, L. *CVXOPT: A Python Package for Convex Optimization*, version 1.1.6, 2013; cvxopt.org.
(79) Painter, J.; Merritt, E. A. mmLib Python Toolkit for Manipulating Annotated Structural Models of Biological Macromolecules. *J. Appl. Crystallogr.* **2004**, *37* (1), 174−178.
(80) Shen, H.; Chou, J. J. MemBrain: Improving the Accuracy of Predicting Transmembrane Helices. *PLoS One* **2008**, *3* (6), No. e2399.
(81) Bray, J. K.; Weiss, D. R.; Levitt, M. Optimized Torsion-Angle Normal Modes Reproduce Conformational Changes More Accurately than Cartesian Modes. *Biophys. J.* **2011**, *101* (12), 2966−2969.
(82) Fisher, R. A. On the Probable Error of a Coefficient of Correlation Deduced from a Small Sample. *Metron* **1921**, *1*, 3−32.
(83) Volkmann, N. Confidence Intervals for Fitting of Atomic Models into Low-Resolution Densities. *Acta Crystallogr., Sect. D: Biol. Crystallogr.* **2009**, *65*, 679−689.
(84) van Zundert, G. C.P.; Bonvin, A. M. J. J. Defining the Limits and Reliability of Rigid-Body Fitting in Cryo-EM Maps Using Multi-Scale Image Pyramids. *J. Struct. Biol.* **2016**, *195* (2), 252−258.

DOI: 10.1021/acs.jmedchem.8b01292
J. Med. Chem. XXXX, XXX, XXX−XXX

(85) Bochevarov, A. D.; Harder, E.; Hughes, T. F.; Greenwood, J. R.; Braden, D. A.; Philipp, D. M.; Rinaldo, D.; Halls, M. D.; Zhang, J.; Friesner, R. A. Jaguar: A High-Performance Quantum Chemistry Software Program with Strengths in Life and Materials Sciences. *Int. J. Quantum Chem.* **2013**, *113* (18), 2110−2142.
(86) Zhao, Y.; Truhlar, D. G. The M06 Suite of Density Functionals for Main Group Thermochemistry, Thermochemical Kinetics, Noncovalent Interactions, Excited States, and Transition Elements: Two New Functionals and Systematic Testing of Four M06 Functionals and 12 Other Functionals. *Theor. Chem. Acc.* **2008**, *119* (5−6), 525−525.
(87) Zhao, Y.; Truhlar, D. G. Density Functionals with Broad Applicability in Chemistry. *Acc. Chem. Res.* **2008**, *41* (2), 157−167.

DOI: 10.1021/acs.jmedchem.8b01292
J. Med. Chem. XXXX, XXX, XXX−XXX